Article

Cell Reports

Inhibition of Lysosome Membrane Recycling Causes Accumulation of Gangliosides that Contribute to Neurodegeneration

Graphical Abstract

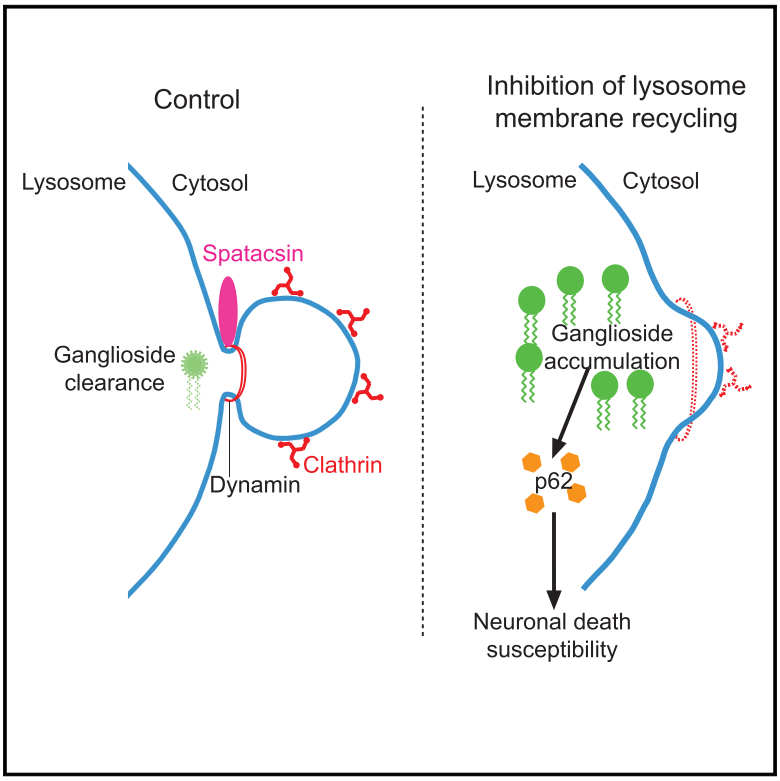

Authors

Maxime Boutry, Julien Branchu, Céline Lustremant, ..., Khalid Hamid El Hachimi, Giovanni Stevanin, Frédéric Darios

Correspondence

giovanni.stevanin@upmc.fr (G.S.), frederic.darios@upmc.fr (F.D.)

In Brief

Boutry et al. show that inhibition of lysosome membrane recycling leads to lysosomal accumulation of some glycosphingolipids (simple gangliosides), which contributes to neuronal death.

Highlights

- Loss of spatacsin promotes accumulation of simple gangliosides in lysosomes
- Inhibition of lysosome membrane recycling leads to accumulation of gangliosides
- Gangliosides promote accumulation of autophagy markers in lysosomes
- Gangliosides contribute to neurodegeneration when lysosome recycling is compromised

Boutry et al., 2018, Cell Reports *23*, 3813–3826
June 26, 2018
https://doi.org/10.1016/j.celrep.2018.05.098

CellPress

Cell Reports
Article

Inhibition of Lysosome Membrane Recycling Causes Accumulation of Gangliosides that Contribute to Neurodegeneration

Maxime Boutry,[1,2,3,4,5,12] Julien Branchu,[1,2,3,4,12] Céline Lustremant,[1,2,3,4] Claire Pujol,[1,2,3,4] Julie Pernelle,[1,2,3,4] Raphaël Matusiak,[1,2,3,4] Alexandre Seyer,[6,13] Marion Poirel,[6] Emeline Chu-Van,[7] Alexandre Pierga,[1,2,3,4] Kostantin Dobrenis,[8] Jean-Philippe Puech,[9] Catherine Caillaud,[9] Alexandra Durr,[1,2,3,4,10] Alexis Brice,[1,2,3,4] Benoit Colsch,[7] Fanny Mochel,[1,2,3,4,10,11] Khalid Hamid El Hachimi,[1,2,3,4,5] Giovanni Stevanin,[1,2,3,4,5,10,*] and Frédéric Darios[1,2,3,4,14,*]

[1]Sorbonne Université, F-75013 Paris, France
[2]Inserm, U1127, F-75013 Paris, France
[3]CNRS, UMR 7225, F-75013 Paris, France
[4]Institut du Cerveau et de la Moelle Epinière (ICM), F-75013 Paris, France
[5]Ecole Pratique des Hautes Etudes, PSL Research University, Laboratoire de Neurogénétique, F-75013 Paris, France
[6]Profilomic SA, F-92100 Boulogne-Billancourt, France
[7]Service de Pharmacologie et d'Immunoanalyse (SPI), Laboratoire d'Etude du Métabolisme des Médicaments, CEA, INRA, Université Paris Saclay, MetaboHUB, F-91191 Gif-sur-Yvette, France
[8]Dominick P. Purpura Department of Neuroscience, Albert Einstein College of Medicine, Bronx, NY 10461, USA
[9]Laboratoire de Biochimie Métabolomique et Protéomique, Hôpital Universitaire Necker-Enfants Malades, AP-HP, F-75015 Paris, France
[10]National Reference Center for Neurogenetic Diseases, Pitié-Salpêtrière University Hospital, APHP, F-75013 Paris, France
[11]Bioclinic and Genetic Unit of Neurometabolic Diseases, Pitié-Salpêtrière University Hospital, F-75013 Paris, France
[12]These authors contributed equally
[13]Present address: MedDay Pharmaceuticals, Paris, France
[14]Lead Contact
*Correspondence: giovanni.stevanin@upmc.fr (G.S.), frederic.darios@upmc.fr (F.D.)
https://doi.org/10.1016/j.celrep.2018.05.098

SUMMARY

Lysosome membrane recycling occurs at the end of the autophagic pathway and requires proteins that are mostly encoded by genes mutated in neurodegenerative diseases. However, its implication in neuronal death is still unclear. Here, we show that spatacsin, which is required for lysosome recycling and whose loss of function leads to hereditary spastic paraplegia 11 (SPG11), promotes clearance of gangliosides from lysosomes in mouse and human SPG11 models. We demonstrate that spatacsin acts downstream of clathrin and recruits dynamin to allow lysosome membrane recycling and clearance of gangliosides from lysosomes. Gangliosides contributed to the accumulation of autophagy markers in lysosomes and to neuronal death. In contrast, decreasing ganglioside synthesis prevented neurodegeneration and improved motor phenotype in a SPG11 zebrafish model. Our work reveals how inhibition of lysosome membrane recycling leads to the deleterious accumulation of gangliosides, linking lysosome recycling to neurodegeneration.

INTRODUCTION

Lysosomes are essential organelles necessary for the degradation of cellular components by the action of hydrolytic enzymes. They are involved in endocytosis and autophagy pathways to promote the degradation of the content of late endosomes and autophagosomes. The degradation step is followed by recycling of structural components into newly forming lysosomes. Under normal conditions, recycling of lysosomal membranes has been proposed to result from the budding of small vesicle carriers from lysosomes (Sridhar et al., 2013). However, under starvation conditions, tubulation occurs in autolysosomes to promote the reformation of new functional lysosomes, a process called autophagic lysosome reformation (ALR) (Yu et al., 2010). The proteins involved in the recycling process include kinesin KIF5B (Du et al., 2016), clathrin, the lipid-modifying enzymes PIP5K1B and PIP5K1A (Rong et al., 2012), spatacsin and spastizin (Chang et al., 2014), members of the AP-2 and AP-4 complex (Rong et al., 2012), dynamin (Schulze et al., 2013), and SPNS1 (Rong et al., 2011). Mutations in the genes encoding the subunits of the AP-4 complex, as well as those encoding spatacsin and spastizin account for severe neurodegenerative disorders, hereditary spastic paraplegias (Tesson et al., 2015). In addition, loss of function of spinster, the *Drosophila* homolog of *SPNS1*, leads to neurodegeneration (Nakano et al., 2001). These data highlight the importance of the lysosome recovery pathway for neuron survival. The accumulation of autolysosomes in neurons of a knockout mouse lacking spatacsin was proposed as evidence that defective autophagic lysosome recovery can contribute to neurodegeneration (Varga et al., 2015). However, the mechanism of ALR has so far only been investigated in cultured non-neuronal cells.

Several of the proteins involved in the recycling of lysosome membranes are directly implicated in membrane curvature, such as clathrin and AP-2 and AP-4 complexes (Rong et al.,

2012). Recently, we implicated the loss of spatacsin, a protein required for the initiation of ALR (Chang et al., 2014), in lysosomal accumulation of lipids in a knockout mouse model (Branchu et al., 2017), therefore linking lysosome membrane recycling to lipid metabolism. Spatacsin is encoded by the *SPG11* gene (Stevanin et al., 2007). Mutations in this gene lead to a spastic gait disorder variably associated with cognitive impairment, peripheral neuropathy, cerebellar ataxia, parkinsonism, and retinal degeneration (Hehr et al., 2007; Stevanin et al., 2007). Knocking out *Spg11* in mice is responsible for early cognitive and motor deficits, consistent with the symptoms observed in the majority of patients with mutations in the *SPG11* gene (Branchu et al., 2017). The accumulation of lipids that was observed in the brain of *Spg11* knockout mice was also detected in post-mortem brain samples of a SPG11 patient (Branchu et al., 2017). However, the mechanisms underlying lipid accumulation and neurodegeneration are unknown.

Here, we show that loss of spatacsin leads to the accumulation of simple gangliosides in lysosomes. The accumulation of gangliosides is a consequence of impaired recycling of lysosomes caused by the absence of functional spatacsin. Decreasing ganglioside levels prevented the accumulation of autophagy markers in lysosomes in cultured neurons, improved neuron survival *in vitro*, and prevented motor phenotype caused by inactivation of *zspg11* in a zebrafish SPG11 model. Our work therefore highlights the importance of lysosome membrane recycling to prevent the detrimental role of gangliosides in neuronal death.

RESULTS

Loss of Spatacsin Promotes the Progressive Accumulation of Gangliosides in Lysosomes in Neurons

Loss of spatacsin in mice leads to lysosomal accumulation of lipids in neurons (Branchu et al., 2017). We investigated the nature of the lipids that accumulate in the cerebral cortex of 8-month-old *Spg11*$^{-/-}$ mice by performing a lipidomic analysis. The levels of free fatty acids, ceramides, and lysophospholipids were significantly lower in the cortex of *Spg11*$^{-/-}$ mice than control mice. Only GM2 ganglioside levels were significantly higher in the cortex of *Spg11*$^{-/-}$ mice than in control mice (Table S1). Immunostaining with a specific antibody showed that GM2 colocalized with lysosomes in *Spg11*$^{-/-}$ mice, from the age of 6 weeks, whereas it was seen as rare small punctae in neurons of control mice (Figure 1A). The proportion of neurons with GM2 staining in lysosomes was higher in *Spg11*$^{-/-}$ than in *Spg11*$^{+/+}$ mice at the age of 6 weeks, and by the age of 8 months, most neurons in motor cortex of *Spg11*$^{-/-}$ mice showed GM2 accumulation (Figure 1B). Quantification of the fluorescence intensity showed that GM2 levels were higher in *Spg11*$^{-/-}$ than *Spg11*$^{+/+}$ cortical neurons at all ages (Figure 1C). GM2 accumulated in large lysosomes in knockout mice as indicated by the colocalization of GM2 and Lamp1 staining (Figure 1A). These data showed that the loss of spatacsin function leads to early and progressive accumulation of the GM2 ganglioside in the lysosomes of neurons in the cerebral cortex. Activity of hexosaminidase A, an enzyme involved in lysosomal catabolism of GM2, was not decreased in cortex extracts obtained from *Spg11*$^{-/-}$ mice compared to controls, suggesting that accumulation of GM2 was not due to an impaired activity of this enzyme (Figure S1A).

Our lipidomic analysis was performed on the whole cortex. It is thus possible that other lipids may accumulate in lysosomes despite the absence of a global change in their levels. Therefore, we purified fractions enriched in lysosomes from the brains of *Spg11*$^{+/+}$ and *Spg11*$^{-/-}$ mice (Figures S1B and S1C), and extracted lipids using the Folch procedure (Folch et al., 1957). Lipidomic analysis was performed on the Folch upper phase, which contains gangliosides. The levels of gangliosides GM2, GM3, GD2, and GD3 were markedly higher in lysosomal fractions obtained from *Spg11*$^{-/-}$ mouse brains than those of control brains (Table 1). We confirmed the enrichment of these gangliosides in lysosomes by immunostaining with specific antibodies (Figures S2A–S2C). Quantification of fluorescence intensity showed that the levels of the four lipid species increased with age and were higher in *Spg11*$^{-/-}$ mouse brains than control brains (Figures 1C–1F). The gangliosides GM3, GD2, and GD3 were colocalized with lysosomes, as GM2 was, consistent with their accumulation in lysosomes. The levels of complex gangliosides (GM1, GD1, and GT1) were slightly, but not significantly higher in the lysosome-enriched fractions (Table 1). Accordingly, there was no difference in the localization of GM1 between *Spg11*$^{+/+}$ and *Spg11*$^{-/-}$ mouse brain as assessed by immunostaining (Figures S2D and S2E).

Loss of Spatacsin Promotes the Early Accumulation of Gangliosides in Lysosomes in Human Neurons

We tested whether the accumulation of gangliosides is also relevant for human pathology using induced pluripotent stem cells (iPSCs) derived from fibroblasts of two independent SPG11 patients and two sex- and age-matched controls. iPSCs of SPG11 patients and healthy subjects that were validated with markers of pluripotency (Figure S3A) were differentiated into brain organoids with predominant cortical identity using a free-floating tridimensional culture method (Paşca et al., 2015). After 90 days of differentiation, the organoids were organized in layers of radial glial cells labeled by Pax6 and Nestin, and peripheral layers of neurons that expressed βIII-tubulin and NeuN (Figure 2A; data not shown). We examined by immunostaining whether gangliosides accumulated in lysosomes in the peripheral layer of neurons (Figures 2B–2F). GM2, GM3, and GD3 showed a punctate immunostaining pattern in the neurons of the peripheral layer of control and SPG11 brain organoids, and the staining largely colocalized with lysosomes in the neurons of the SPG11 brain organoids (Figures 2B and S3B–S3D). Quantification of fluorescence intensity showed GM2 and GM3 levels to be higher in SPG11 cortical organoids than control organoids (Figures 2C–2F). Furthermore, the variance of the fluorescence intensity of GM2, GM3, and GD3 staining was also higher in organoids derived from SPG11 patients than those derived from healthy controls, consistent with their accumulation in lysosomes. There was no difference in GD2 staining between organoids derived from SPG11 patients and healthy controls, in agreement with the lack of a difference in GD2 staining in the cortices of *Spg11*$^{+/+}$ and *Spg11*$^{-/-}$ mice at early stages (Figure 1E). Overall, these data show that simple gangliosides accumulated in lysosomes of the human neurons, starting at early

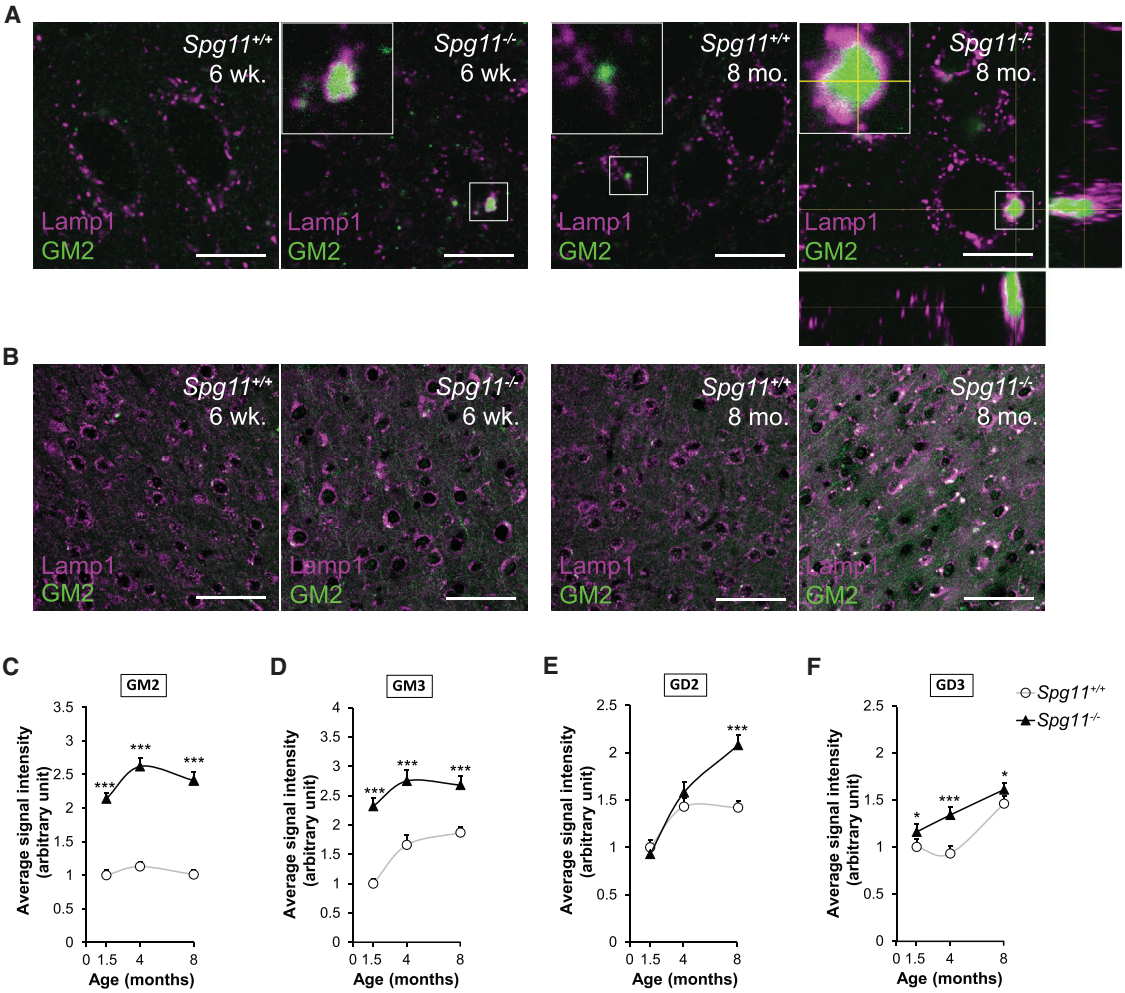

Figure 1. Spatacsin Loss Promotes Lysosomal Accumulation of Gangliosides in Neurons of the Cortex

(A and B) GM2 (green) and Lamp1 (magenta) immunostaining of *Spg11*$^{+/+}$ and *Spg11*$^{-/-}$ neurons of the layer V of the motor cortex from 6-week-old and 8-month-old mice observed by confocal microscopy with a 60× (A) or 20× (B) objective. Images showing the accumulation of GM2-positive staining in lysosomes surrounded by Lamp1 staining in 6-week-old and 8-month-old *Spg11*$^{-/-}$ animals. Insets show the view along the z axis (A). Scale bars: 10 μm (A) and 50 μm (B). (C–F) Quantification of the mean of the GM2 (C), GM3 (D), GD2 (E), and GD3 (F) immunostaining intensity per neuron. Quantification was performed in neurons of the layer V of motor cortex that were detected by their large soma. The graphs show the mean ± SEM values. N = 10–15 neurons quantified per cortex slices in five cortex slices of five independent mice. Differences between *Spg11*$^{+/+}$ and *Spg11*$^{-/-}$ were analyzed by a Kruskal-Wallis test at each time point; * $p \leq 0.05$, *** $p \leq 0.0001$.

See also Table S1 and Figures S1 and S2.

stages of development represented by the cortical organoid model (Paşca et al., 2015). This prompted us to investigate how spatacsin regulates the levels of gangliosides in lysosomes.

Spatacsin Is Recruited to Lysosomes Containing Gangliosides in Primary Cultures of Cortical Neurons

We analyzed whether gangliosides accumulated in lysosomes of primary cultures of cortical neurons derived from *Spg11*$^{-/-}$ mouse embryos. By immunostaining, GM2, GM3, GD2, and GD3 significantly accumulated in lysosomes in cultured neurons derived from *Spg11*$^{-/-}$ embryos (Figures 3A–3E and S4A–S4C). Primary cultures of cortical neurons are thus a good model to investigate the mechanisms leading to ganglioside accumulation in lysosomes. GM2 was the ganglioside that accumulated the most in lysosomes, and lipidomic analysis showed higher levels of GM2 in *Spg11*$^{-/-}$ than in *Spg11*$^{+/+}$ neurons (Figure S4D). We therefore used it as a marker for ganglioside accumulation in subsequent experiments.

We investigated the role of spatacsin in ganglioside metabolism by transfecting neurons with a V5-tagged spatacsin. In control conditions, the protein had a diffuse localization throughout the cytoplasm. However, it was partially colocalized with the few GM2-positive lysosomes in these cells (Figure 3F). To investigate the link between gangliosides and spatacsin, we enforced accumulation of gangliosides in lysosomes by downregulating the expression of neuraminidase 1 (Neu1), an enzyme

Table 1. Relative Amounts of Various Classes of Gangliosides in Lysosome-Enriched Fractions Obtained from the Brains of 8-Month-Old *Spg11*$^{+/+}$ and *Spg11*$^{-/-}$ Mice

	Spg11$^{+/+}$	*Spg11*$^{-/-}$	Fold Change
GM3	N = 8	N = 7	–
GM3 (d18:1/18:1)	14.2 ± 3.1	42.3 ± 5.3[a]	2.98
GM3 (d18:1/18:0)	518.2 ± 89.5	1,316.6 ± 194.1[a]	2.54
GM3 (d18:1/20:0)	51.1 ± 8.7	170.3 ± 24.5[a]	3.34
GM2			
GM2 (d18:1/18:0)	286.5 ± 46.3	957.6 ± 119.5[a]	3.34
GM2 (d18:1/20:0)	68.9 ± 12.3	296.9 ± 40.9[a]	4.31
GD3			
GD3 (d18:1/18:0)	155.8 ± 23.9	321.0 ± 45.2[a]	2.06
GD3 (d18:1/18:0)	139.8 ± 26.7	307.7 ± 41.0[a]	2.20
GD3 (d18:1/20:0)	39.9 ± 8.5	87.1 ± 12.3[a]	2.18
GD2			
GD2 (d18:1/18:0)	53.1 ± 8.4	145.3 ± 22.7[a]	2.73
GD2 (d18:1/20:0)	54.7 ± 10.9	159.9 ± 24.2[a]	2.93
GM1			
GM1 (d18:1/18:1)	52.8 ± 11.7	84.9 ± 10.7	1.61
GM1 (d18:1/18:0)	478.8 ± 87.2	778.7 ± 91.5	1.63
GM1 (d18:1/20:0)	198.6 ± 40.5	322.3 ± 42.7	1.62
GD1			
GD1 (d18:1/18:1)	280.2 ± 65.6	338.4 ± 40.1	1.21
GD1 (d18:1/18:0)	4,025.6 ± 1221.1	4,648.3 ± 615.8	1.15
OAc-GD1 (d18:1/18:0)	174.3 ± 39.3	222.2 ± 19.0	1.27
GD1 (d18:1/20:0)	1,653.3 ± 404.0	1,781.7 ± 225.9	1.08
GT1			
GT1 (d18:1/18:0)	493.4 ± 174.0	535.5 ± 74.3	1.09
OAc-GT1 (d18:1/18:0)	192.9 ± 60.9	243.4 ± 34.1	1.26
GT1 (d18:1/20:0)	220.6 ± 74.7	230.1 ± 32.5	1.04
OAc-GT1 (d18:1/20:0)	140.8 ± 37.8	163.7 ± 23.7	1.16

Arbitrary units, normalized to lysosomal protein concentration.
[a]$p < 0.05$, t test with Benjamini-Hochberg procedure to correct for multiple testing.

involved in the lysosomal degradation of gangliosides (Bonten et al., 1996). We used two independent microRNA (miRNA) sequences that efficiently downregulated Neu1 expression (Figure S4E). Downregulation of Neu1 promoted significant accumulation of GM2 in lysosomes in transfected *Spg11*$^{+/+}$ and *Spg11*$^{-/-}$ neurons (Figures S4F and S4G), suggesting that neuraminidase activity and lysosome membrane recycling are independent pathways to clear gangliosides. In wild-type neurons that were transfected with both a miRNA targeting Neu1 and expressing V5-tagged spatacsin, the latter was strongly enriched in GM2-positive lysosomes (Figure 3F), suggesting that spatacsin is recruited to lysosomes containing gangliosides.

Lysosome Membrane Recycling Promotes Ganglioside Clearance from Lysosomes

Loss of spatacsin in fibroblasts is responsible for the presence of large lysosomes (Renvoisé et al., 2014). This phenotype is the consequence of impaired lysosome recycling analyzed in cell lines by monitoring the formation of tubules emanating from Lamp1-positive vesicles by live imaging (Chang et al., 2014). In cultured neurons, we did not detect tubules emanating from lysosomes by live imaging (Figure S5A), even with treatment such as dynasore, a dynamin inhibitor that enhances the number of lysosomal tubules in fibroblasts (Chang et al., 2014). However, we observed that the average number of lysosomes immunostained with Lamp1 and with an apparent diameter larger than 1 μm was higher in *Spg11*$^{-/-}$ neurons than in control neurons (Figure 3G). We evaluated the role of gangliosides in the formation of large lysosomes using miglustat, which inhibits glucosylceramide synthase, an early step in glycosphingolipid synthesis, and is known to decrease GM2 levels in a model of Sandhoff disease (Jeyakumar et al., 1999). In primary cultures of cortical neurons, miglustat significantly decreased the levels of GM2 in a dose-dependent manner (Figures S5B and S5C), but it did not change the number of large lysosomes (Figure 3G). To confirm these data, we used two independent miRNAs that target GM3

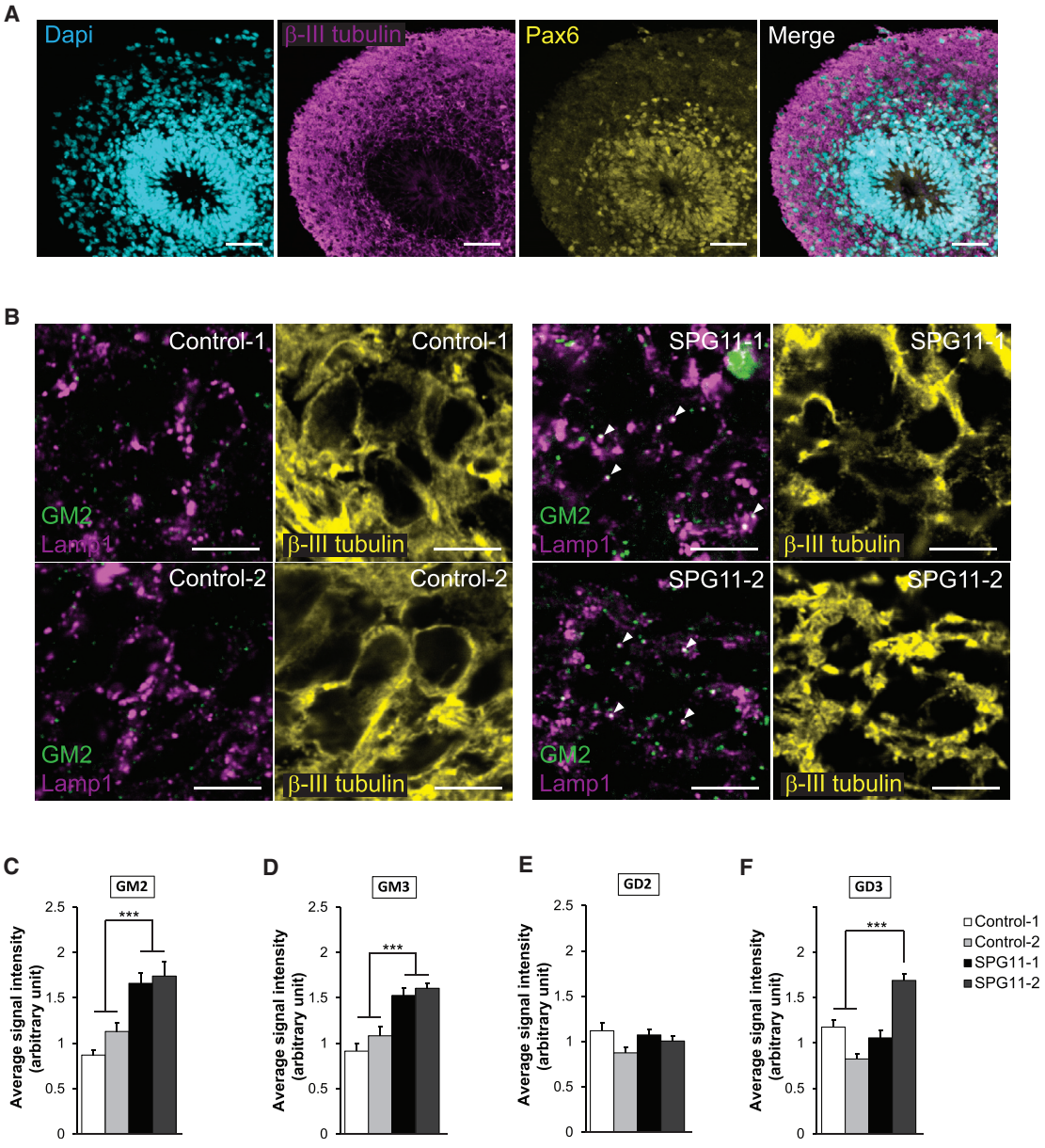

Figure 2. Spatacsin Loss Promotes Lysosomal Accumulation of Gangliosides in Neurons Derived from SPG11 Patients

(A) Immunostaining of brain organoids differentiated for 90 days *in vitro* with antibodies against the progenitor marker Pax6 and the neuron-specific marker βIII-tubulin. Note that neuronal cells are concentrated at the periphery of the organoids. Scale bar: 50 μm.

(B) GM2 (green) and Lamp1 (magenta) immunostaining in the neuronal layer of organoids derived from healthy subjects or SPG11 patients. βIII-Tubulin (yellow) shows the neuronal identity of the cells that were analyzed. Confocal microscopy images showing the accumulation of GM2-positive staining in lysosomes labeled by Lamp1 staining of organoids derived from SPG11 patients (arrowheads). Scale bar: 10 μm.

(C–F) Quantification of the mean of the GM2 (C), GM3 (D), GD2 (E), and GD3 (F) immunostaining intensity per neuron. The graph shows mean ± SEM values. N = 10–15 neurons quantified per slices in five slices obtained from three independent organoids. One-way ANOVA; ***$p \leq 0.001$.

See also Figure S3.

synthase, the enzyme producing the first ganglioside in the biosynthetic pathway, and from which all other sialylated gangliosides are generated (Xu et al., 2010). Expression of these miRNAs significantly decreased the expression of GM3 synthase mRNA and GM2 levels (Figures S5D–S5F). The number of large lysosomes was unchanged when GM3 synthase was downregulated in *Spg11*$^{+/+}$ and *Spg11*$^{-/-}$ neurons (Figure S5G). This indicates that accumulation of large lysosomes does not depend on *de novo* synthesis of gangliosides. We thus hypothesized that the accumulation of GM2 in lysosomes occurs as a consequence of inhibition of lysosome membrane recycling in *Spg11*$^{-/-}$ cells.

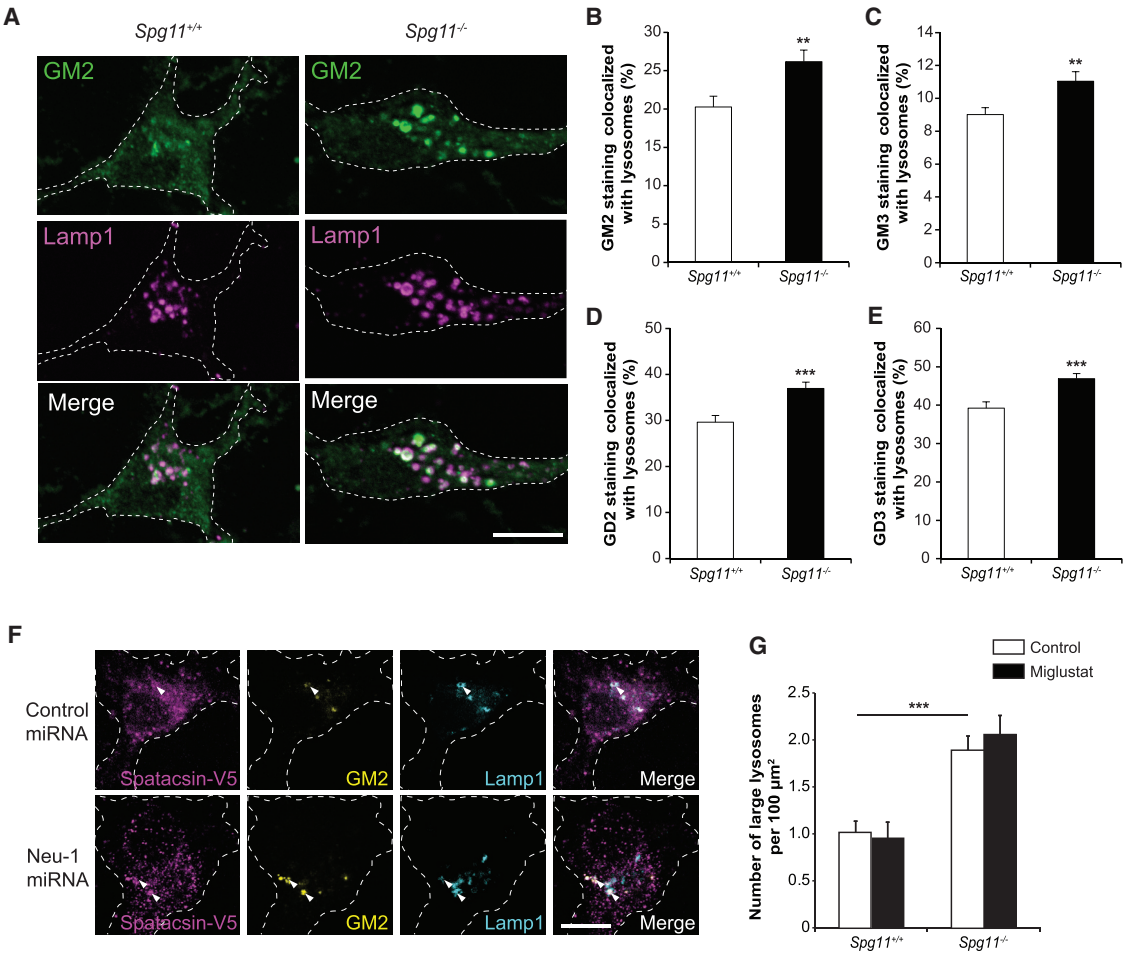

Figure 3. Spatacsin Loss Induces Lysosomal Accumulation of Gangliosides in Primary Cultures of Mouse Cortical Neurons

(A) GM2 (green) and Lamp1 (magenta) immunostaining of *Spg11*$^{+/+}$ and *Spg11*$^{-/-}$ neurons cultured for 6 days *in vitro*. Confocal microscopy images showing the accumulation of GM2-positive staining of lysosomes labeled by Lamp1 staining. Scale bar: 10 μm.

(B–E) Quantification of the proportion of GM2 (B), GM3 (C), GD2 (D), and GD3 (E) staining that is localized in lysosomes. The graphs show the mean ± SEM values. N = 58–71 neurons quantified in three independent neuron preparations. t test; **p ≤ 0.01 and ***p ≤ 0.001.

(F) Immunostaining of GM2 ganglioside (green), Lamp1 (cyan), and Spatacsin-V5 (magenta) in wild-type neurons co-transfected with vectors allowing expression of Spatacsin-V5 and either control miRNA or miRNA downregulating Neu1. Spatacsin is enriched around GM2-positive vesicles (arrowheads). Scale bar: 10 μm.

(G) Quantification of the number of lysosomes detected with Lamp1 immunostaining and with a diameter larger than 1 μm in *Spg11*$^{+/+}$ and *Spg11*$^{-/-}$ neurons cultured for 6 days *in vitro* and treated or not with miglustat (100 μM). The graphs show the mean ± SEM values. N = 62–64 neurons quantified in four independent neuron preparations (control); N = 24–34 neurons quantified in three independent neuron preparations (miglustat). One-way ANOVA, followed by Holm-Sidak post hoc test; ***p ≤ 0.001.

See also Figure S4.

To test this hypothesis, we analyzed the role of clathrin, one of the proteins required for recycling of lysosome membrane (Rong et al., 2012). Downregulation of clathrin levels using two independent miRNAs (Figures S5H and S5I) led to higher number of large lysosomes per neurons (Figure 4A). Inhibition of lysosome membrane recycling following clathrin downregulation was associated with a higher amount of GM2 ganglioside in lysosomes (Figure 4B), suggesting that inhibition of lysosome membrane recycling prevented or slowed down clearance of gangliosides. In *Spg11*$^{-/-}$ neurons, clathrin colocalized with lysosomes containing high amounts of the GM2 ganglioside (Figure 4C). The proportion of cellular clathrin colocalized with the GM2 was higher in *Spg11*$^{-/-}$ neurons than control neurons (Figure 4D). Accordingly, clathrin staining was high for large autofluorescent lysosomes that contain high amounts of GM2 (Figure 1A) in the brains of *Spg11*$^{-/-}$ mice (Figure 4E). This suggests that clearance of gangliosides was blocked downstream of clathrin recruitment in the absence of spatacsin.

In a two-hybrid screen, we found that dynamin-1, a homolog of dynamin-2 that is important for termination of the lysosome recycling (Schulze et al., 2013), is a putative interactor of the C-terminal domain of spatacsin. We validated this interaction by co-immunoprecipitation in HeLa cells (Figure 4F). We analyzed

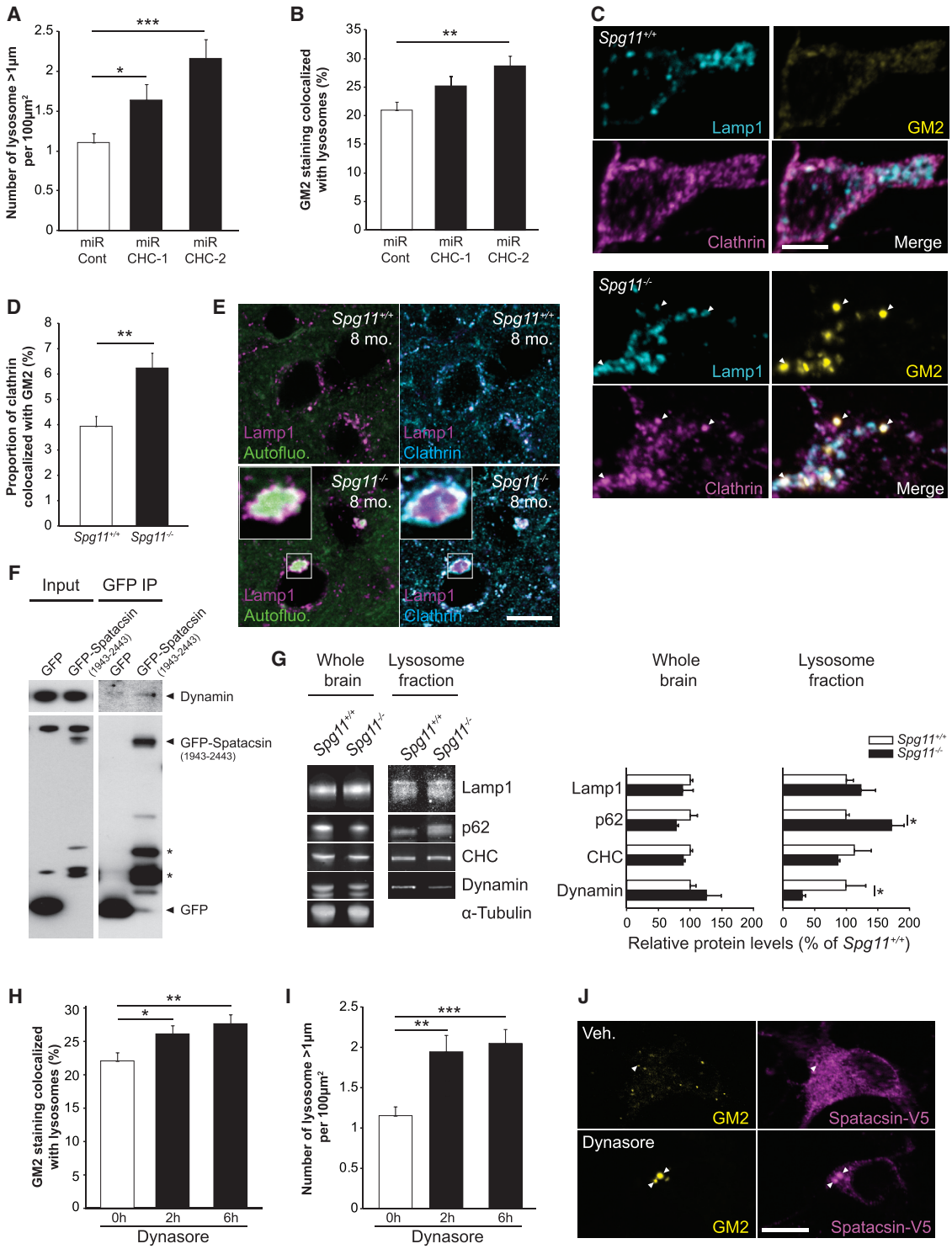

Figure 4. Spatacsin Promotes Clearance of Gangliosides from Lysosomes

(A) Quantification of the number of lysosomes with a diameter larger than 1 μm in *Spg11*$^{+/+}$ and *Spg11*$^{-/-}$ neurons expressing control miRNA or miRNA downregulating clathrin heavy chain (CHC). The graphs show the mean ± SEM values. N = 35–50 neurons quantified in two independent neuron preparations. One-way ANOVA, followed by Holm-Sidak post hoc test; *p = 0.03 and ***p ≤ 0.001.

(B) Quantification of the proportion of GM2 staining that is localized in lysosomes. The graphs show the mean ± SEM values. N = 36–49 neurons quantified in two independent neuron preparations. One-way ANOVA, followed by Holm-Sidak post hoc test; **p = 0.0017.

(legend continued on next page)

whether the absence of spatacsin had an impact on dynamin recruitment to lysosomes. Western blot performed on the lysosome-enriched fractions that were used for lipidomic analysis (Table 1) showed that dynamin was markedly less abundant in lysosome fractions obtained from *Spg11*$^{-/-}$ than *Spg11*$^{+/+}$ mouse brains (Figure 4G), while no difference was observed in whole-brain extracts. Immunostaining on cultured neurons showed a decreased amount of dynamin colocalized with Lamp1-positive lysosomes in *Spg11*$^{-/-}$ than *Spg11*$^{+/+}$ neurons (Figure S5J). These results, together with the enrichment of spatacsin on lysosomes containing GM2 (Figure 3F), led us to hypothesize that spatacsin participates in recruitment of dynamin to lysosomes to clear gangliosides. To test this hypothesis, we inhibited dynamins using dynasore treatment, which promoted higher levels of GM2 in lysosomes (Figure 4H). Furthermore, dynasore treatment in control neurons increased the number of large lysosomes (Figure 4I), consistent with the role of dynamin in late step of lysosome membrane recycling. Dynasore also led to the enrichment of V5-spatacsin in lysosomes containing GM2 (Figure 4J), suggesting that spatacsin is implicated upstream of dynamin. Altogether, these data suggest that the machinery implicated in lysosome membrane recycling in fibroblasts is used by neurons to clear gangliosides from lysosomes.

High Levels of Gangliosides in Lysosomes Contribute to the Accumulation of Autophagy Markers in Lysosomes

We then investigated the consequences of ganglioside accumulation on lysosome function. Catalytic activity monitored by the Magic red cathepsin B substrate was not altered in *Spg11*$^{-/-}$ neurons (Figure S6A), suggesting that it was not altered by accumulation of gangliosides. Loss of spatacsin was shown to result in accumulation of autolysosomes (Chang et al., 2014; Varga et al., 2015). Accordingly, even if the global levels of the autophagy marker p62 were similar in total brain extracts of 8-month-old *Spg11*$^{-/-}$ and *Spg11*$^{+/+}$ mice, p62 was more abundant in lysosome-enriched fractions obtained from *Spg11*$^{-/-}$ than *Spg11*$^{+/+}$ mouse brains (Figure 4G). Similarly, in primary cultures of neurons, the proportion of lysosomes that were positive for the autophagic marker p62, was higher in *Spg11*$^{-/-}$ neurons than in control neurons, and this proportion increased over time in cultured *Spg11*$^{-/-}$ neurons (Figure 5A). We then investigated whether GM2 contributed to increase the proportion of lysosomes containing p62 marker. Close examination of GM2 staining in neurons showed that it mainly accumulated in a subset of lysosomes that were also stained with p62 (Figure 5B). The proportion of lysosomes stained with p62 and GM2 antibodies was higher in *Spg11*$^{-/-}$ neurons than in control neurons and increased over time (Figure 5C), suggesting that GM2 accumulation might contribute to the increase in lysosomes displaying autophagy markers.

To test this hypothesis, we decreased the amount of gangliosides in lysosomes using miglustat (100 μM), or by downregulating GM3 synthase (Figures S5D–S5F). This strongly decreased the proportion of lysosomes positive for the p62 marker in *Spg11*$^{-/-}$ neurons (Figures 5D and 5E). Overall, our data suggest that the accumulation of GM2 in lysosomes prevents the degradation of their content. Conversely, we enforced accumulation of GM2 in lysosomes by downregulation of the expression of Neu1. This resulted in a significant increase in the proportion of lysosomes positive for the autophagic marker p62 (Figure 5F). Together, these data suggest that ganglioside accumulation leads to the accumulation of the autophagy marker p62 in lysosomes.

Gangliosides Contribute to Neurodegeneration in Cultured Neurons

We then investigated whether accumulation of gangliosides contribute to neurodegeneration using primary cultures of mouse cortical neurons. Basal neuronal death was similar in *Spg11*$^{+/+}$ and *Spg11*$^{-/-}$ neurons (Figures 6A and 6B). We thus evaluated neuronal death triggered by glutamate, which occurs in many models of neurodegenerative diseases (Lewerenz and Maher, 2015) and was shown to increase ganglioside levels in cultured neurons (Park et al., 2016). Accordingly, we observed a moderate, but statistically significant, increase in overall GM2 immunoreactivity, both in control and *Spg11*$^{-/-}$ neurons (Figure S6B).

Neuronal death triggered by glutamate was significantly higher in neurons obtained from *Spg11*$^{-/-}$ embryos than

(C) Immunostaining of *Spg11*$^{-/-}$ neurons with Lamp1 (cyan), GM2 (yellow), and clathrin (magenta) antibodies. Arrowheads point to lysosomes positive for the GM2 marker that also show recruitment of clathrin. Scale bar: 5 μm.
(D) Quantification of the proportion of clathrin colocalized with GM2-positive vesicles. The graphs show the mean ± SEM values. N = 88 (*Spg11*$^{+/+}$) and 102 (*Spg11*$^{-/-}$) neurons quantified in three independent neuron preparations. t test; **p = 0.0023.
(E) Confocal microscopy images of autofluorescence (green), Lamp1 (magenta), and clathrin (cyan) immunostaining of *Spg11*$^{+/+}$ and *Spg11*$^{-/-}$ cortical motor neurons from 8-month-old animals showing the accumulation of clathrin surrounding autofluorescent lysosomes. Scale bars: 10 μm.
(F) Western blot showing the interaction of GFP-spatacsin (domain 1943–2443) with dynamin in HeLa cells expressing GFP or GFP-spatacsin 1943–2443. Western blot signals were detected by chemiluminescence.
(G) Left: western blots showing the relative amount of Lamp1, p62, clathrin heavy chain (CHC), and dynamin in whole-brain lysates and lysosome-enriched fractions obtained from *Spg11*$^{+/+}$ and *Spg11*$^{-/-}$ mouse brains. Western blot signals were detected using an infrared imaging system. Right: relative quantification of the band intensities. The graphs show the mean ± SEM. Preparations from N = 3 independent animals. One-tailed Mann-Whitney U test; *p = 0.05.
(H) Quantification of the proportion of GM2 staining that is localized in lysosomes in neurons treated with 40 μM dynasore. The graphs show the mean ± SEM values. N = 73–124 neurons quantified in three independent neuron preparations. One-way ANOVA, followed by Holm-Sidak post hoc test; *p = 0.02 and **p = 0.01.
(I) Quantification of the number of lysosomes with a diameter larger than 1 μm in neurons treated with 40 μM dynasore. The graphs show the mean ± SEM values. N = 49–54 neurons quantified in two independent neuron preparations. One-way ANOVA, followed by Holm-Sidak post hoc test; **p = 0.001 and ***p ≤ 0.001.
(J) Immunostaining of GM2 ganglioside (yellow) and Spatacsin-V5 (magenta) in neurons transfected with vector allowing expression of Spatacsin-V5 and treated with either vehicle or dynasore (40 μM) for 2 hr. Spatacsin is enriched around GM2-positive vesicles (arrowheads). Scale bar: 10 μm.
See also Figure S5.

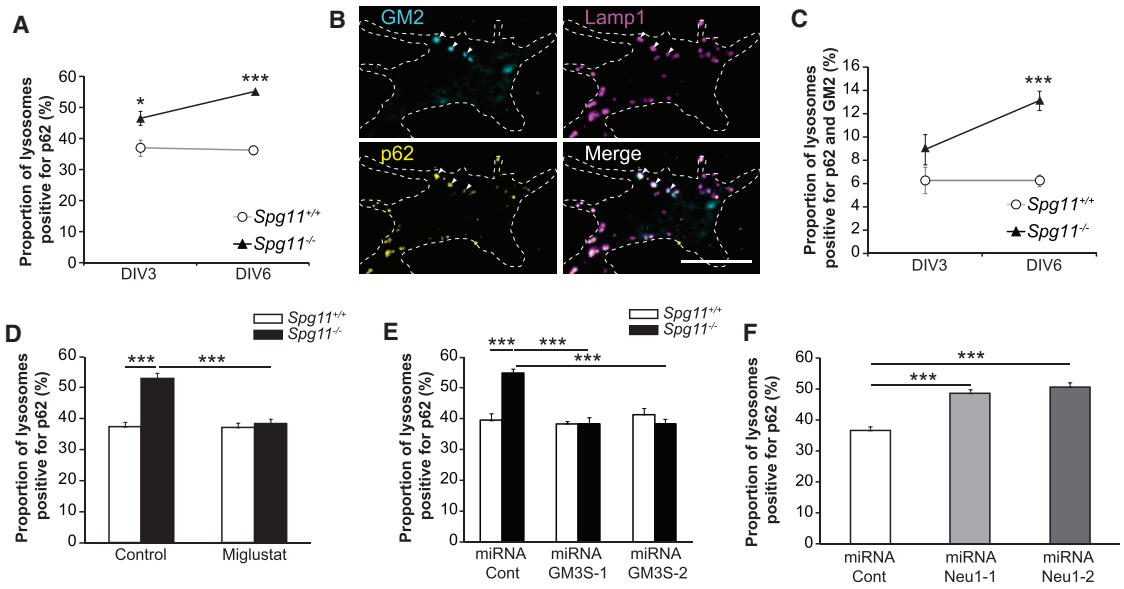

Figure 5. GM2 Accumulation in Lysosomes Promotes the Accumulation of Autophagy Marker p62 in Lysosomes

(A) Proportion of lysosomes stained with Lamp1 that were also positive for p62 in *Spg11*$^{+/+}$ and *Spg11*$^{-/-}$ neurons after 3 and 6 days *in vitro*. The graph shows the mean ± SEM values. Two-way ANOVA, followed by Holm-Sidak post hoc test; *p = 0.04 and ***p < 0.001.

(B) Immunostaining of *Spg11*$^{-/-}$ neurons with GM2 antibody (cyan), lysosomal marker Lamp1 (magenta), and the autophagy marker p62 (yellow). Arrowheads indicate lysosomes, which were positive for p62 and GM2 staining. Scale bar: 10 μm.

(C) Proportion of lysosomes stained with Lamp1 that were also positive for both p62 and GM2 in *Spg11*$^{+/+}$ and *Spg11*$^{-/-}$ neurons after 3 and 6 days *in vitro*. The graph shows the mean ± SEM values. Two-way ANOVA, followed by Holm-Sidak post hoc test; ***p < 0.001.

(D) Effect of miglustat treatment (100 μM) on the proportion of lysosomes stained with Lamp1 that were also positive for p62 in *Spg11*$^{+/+}$ and *Spg11*$^{-/-}$ neurons after 6 days *in vitro*. The graph shows the mean ± SEM values. Two-way ANOVA, followed by Holm-Sidak post hoc test; ***p < 0.001.

(E) Effect of the downregulation of GM3 synthase with two independent miRNAs (GM3S-1 and GM3S-2) on the proportion of lysosomes stained with Lamp1 that were also positive for p62 in control neurons after 6 days *in vitro*. The graph shows the mean ± SEM values. Two-way ANOVA, followed by Holm-Sidak post hoc test; ***p < 0.001.

(F) Effect of Neu1 downregulation with two independent miRNAs (Neu1-1 and Neu1-2) on the proportion of lysosomes stained with Lamp1 that were also positive for p62 in control neurons after 6 days *in vitro*. The graph shows the mean ± SEM values. One-way ANOVA, followed by Holm-Sidak post hoc test; ***p < 0.001.

In (A–D), day *in vitro* 3 (DIV3), N = 47–50 neurons quantified in two independent neuron preparations; DIV6, N = 173–193 neurons quantified in four independent neuron preparations. In (E), N = 7–29 neurons quantified in two independent neuron preparations. In (F), N = 57–68 neurons quantified in three independent neuron preparations.

control neurons (Figures 6A and 6B). Miglustat treatment of *Spg11*$^{-/-}$ neurons decreased glutamate-induced neuronal death in a dose-dependent manner (Figure 6A). Similar data were obtained when GM2 levels were decreased after downregulation of GM3 synthase (Figure 6B). These data suggest that GM2 accumulation contributes to neuronal death. We confirmed this hypothesis by inducing the accumulation of gangliosides in lysosomes, after downregulating Neu1, and monitoring neuronal death triggered by glutamate. Increasing ganglioside levels sensitized the neurons to glutamate-triggered cell death (Figure 6C).

We monitored p62 levels in control and *Spg11*$^{-/-}$ neurons treated with glutamate to determine whether ganglioside-mediated accumulation of autophagy markers in lysosomes contributed to glutamate-induced neuronal death. We observed no difference in p62 levels in untreated neurons. In contrast, glutamate treatment significantly increased p62 levels in *Spg11*$^{-/-}$ neurons, which was inhibited when ganglioside levels were decreased by miglustat treatment (Figure S6C). These data suggest that gangliosides contribute to neuronal death by promoting the accumulation of the autophagy marker p62.

Inhibition of Ganglioside Synthesis in Zebrafish Rescues the Motor Dysfunction Induced by Loss of Spatacsin

Finally, we tested the pathological role of ganglioside accumulation in an *in vivo* model. Since gangliosides accumulate in lysosomes at embryonic stages, we inhibited spatacsin expression in zebrafish larvae using injection of antisense morpholinos, which leads to a motor phenotype (Martin et al., 2012). Zebrafish larvae injected with *zspg11* antisense morpholinos had a stronger GM2 staining in the telencephalon than larvae injected with mismatch morpholinos, as assessed by immunostaining. The stronger staining with GM2 antibody was corrected in larvae treated by miglustat (Figures 6D and 6E). We therefore were able to monitor the role of gangliosides in the motor phenotype in this model. Larvae injected with *zspg11* antisense morpholinos presented with a motor phenotype that was characterized by either a loss of motility or a paralysis (Figure 6F) that was rarely or never observed in larvae injected with a mismatch morpholino or in uninjected larvae, respectively. When larvae were treated with miglustat, the proportion of paralyzed larvae was significantly reduced in a dose-dependent manner compared to controls (Figure 6F). To confirm these data, we monitored the

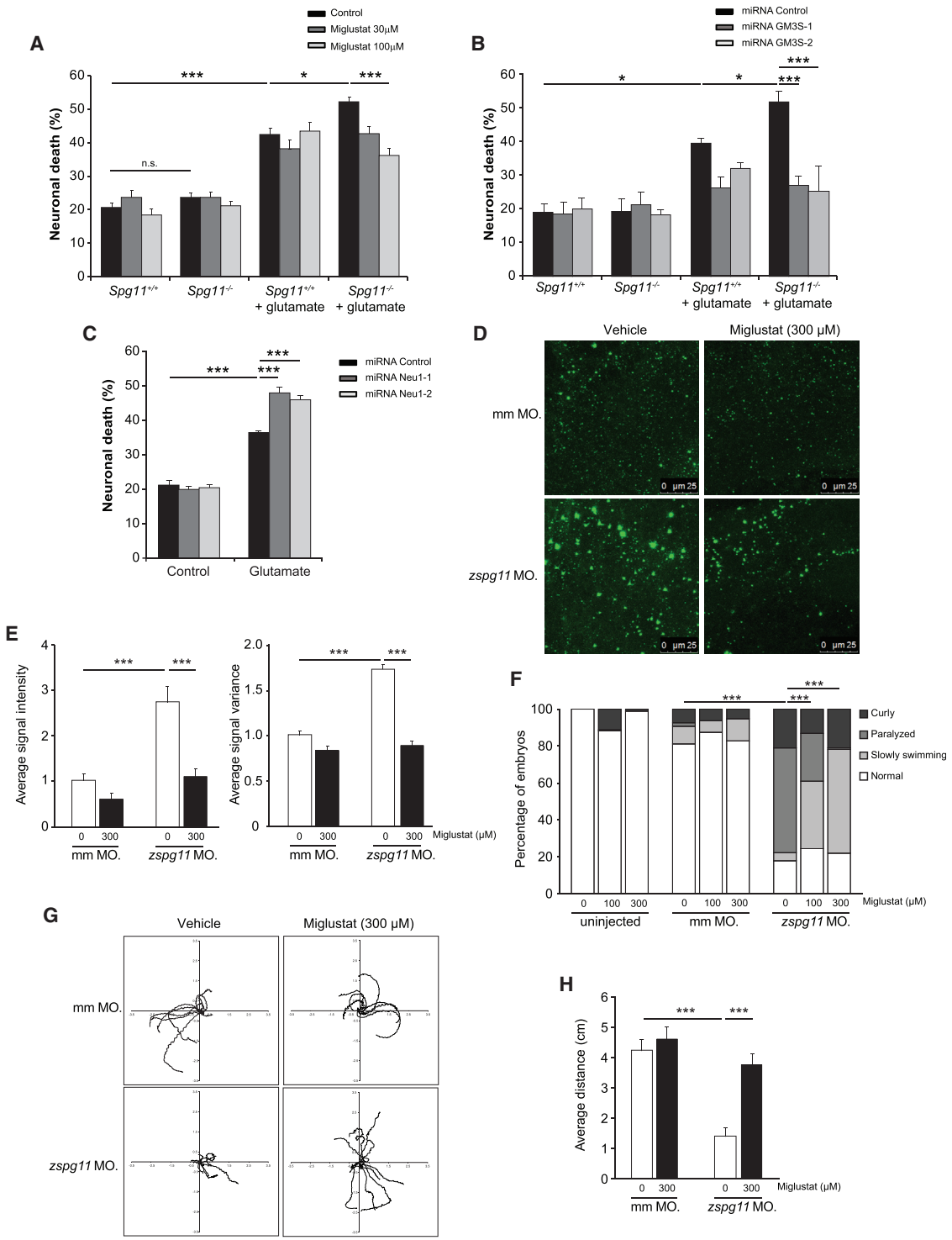

Figure 6. Decreasing Ganglioside Synthesis Prevents Neuronal Death and Improves Motor Dysfunction in Zebrafish Deficient for Spatacsin and Modeling SPG11

(A) Quantification of neuronal death 30 hr after incubation of neurons with glutamate (200 μM) in primary cultures of *Spg11*$^{+/+}$ or *Spg11*$^{-/-}$ cortical neurons treated with miglustat. The graph shows the mean ± SEM values. N = 5–14 independent experiments. One-way ANOVA, followed by Holm-Sidak post hoc test; *p = 0.002 and ***p < 0.001.

(B) Quantification of neuronal death 30 hr after incubation of neurons with glutamate (200 μM) in primary cultures of *Spg11*$^{+/+}$ and *Spg11*$^{-/-}$ cortical neurons transfected with vectors expressing control miRNA or two different miRNAs against GM3 synthase. The graph shows the mean ± SEM. N = 3–8 independent experiments. One-way ANOVA, followed by Holm-Sidak post hoc test; *p < 0.02 and ***p < 0.001.

(legend continued on next page)

distance traveled by larvae following a touch-evoked escape response. Morphants injected with *zspg11* antisense morpholinos showed significantly shorter touch-induced escapes than larvae injected with control morpholinos (Videos S1 and S2). This phenotype was significantly corrected when larvae were treated with miglustat (Figures 6G and 6H; Video S3), while miglustat had no effect on morphants injected with mismatch morpholino. Together, these data demonstrate the deleterious role of gangliosides in an *in vivo* model of the SPG11 pathology.

DISCUSSION

Using models of hereditary spastic paraplegia caused by mutations in the *SPG11* gene, as well as inhibition of proteins implicated in ALR, we show that impairment of lysosome membrane recycling in neurons leads to accumulation of gangliosides in lysosomes, thereby contributing to neurodegeneration.

The recycling of lysosomal membranes has been mainly investigated in cultured cell lines or fibroblasts, and few data are available in neuronal models. Loss of spatacsin leads to accumulation of autolysosomes and depletion of lysosomes in the brain of an *Spg11* knockout mouse model (Varga et al., 2015), but the molecular mechanisms underlying this phenomenon have not been entirely elucidated. ALR described in cell lines occurs after the induction of autophagy and leads to the formation of tubules extruding from autolysosomes (Chang et al., 2014; Yu et al., 2010). In neurons, we were unable to promote autophagy following starvation, as previously observed (Mizushima et al., 2004), and did not observe tubules extruding from lysosomes. In nutrient-rich conditions, lysosome recycling mainly occurs via vesiculation, a mechanism implicating notably the phosphoinositide kinase PI4KB and clathrin (Sridhar et al., 2013). Spatacsin interacts with PI4KB and was proposed to participate in lysosome vesiculation in nutrient-rich conditions (Chang et al., 2014). The presence of large lysosomes observed in neurons when spatacsin is absent or when clathrin or dynamin are inhibited could thus be a consequence of impaired recycling of lysosomal membrane mediated by vesiculation.

The loss of spatacsin leads to a strong accumulation of gangliosides in lysosomes in the cerebral cortex of mice, which increased with age, but was not due to impairment of hexosaminidase A activity. Gangliosides are normally degraded into ceramide and sialic acid in lysosomes, and these metabolites are transported to the endoplasmic reticulum (Tettamanti et al., 2003). Our lipidomic data showed that the accumulation of gangliosides is paralleled by a decrease in ceramide, which could be a consequence of impaired ganglioside clearance from lysosomes. The implication of spatacsin in initiation of lysosome membrane recycling (Chang et al., 2014) led us to hypothesize that recycling of lysosome membrane could contribute to clear gangliosides from lysosomes. This is supported by the accumulation of gangliosides observed when lysosome membrane recycling is inhibited by downregulation of clathrin or inhibition of dynamin. The coimmunoprecipitation of spatacsin with dynamin, and the decreased amount of dynamin in lysosomes in the absence of spatacsin, suggests that spatacsin recruits dynamin to this subcellular compartment. Thus, spatacsin, besides its role in initiation of lysosome membrane recycling (Chang et al., 2014), could contribute to the late stage of recycling by recruiting dynamin to promote fission and release membrane from lysosomes. Impaired vesicle fission and accumulation of clathrin-coated buds have been observed in cortical granules of oocytes in the *souffle* zebrafish mutant that has no spastizin (Kanagaraj et al., 2014). Spastizin is a spatacsin interactor implicated in lysosome membrane recycling (Chang et al., 2014). Its expression is strongly decreased in the brain of *Spg11*$^{-/-}$ mice (Branchu et al., 2017), which could also contribute to impaired lysosomal membrane recycling. Our data therefore suggest that, in the absence of spatacsin, impaired lysosome membrane recycling leads to the progressive accumulation of gangliosides in lysosomes as the disease progresses.

Inhibition of ganglioside synthesis prevented neuronal death *in vitro* but did not compensate for the formation of large lysosomes, suggesting that inhibition of lysosome membrane recycling itself is not responsible for neurodegeneration. In contrast, modulation of ganglioside synthesis showed that these molecules contribute to the accumulation of the autophagy marker p62 in lysosomes. The catalytic activity of the lysosomal protease cathepsin B was not altered in *Spg11*$^{-/-}$ neurons, but the accumulation of gangliosides could slightly impair other lysosomal activities leading to progressive accumulation of autophagic markers in lysosomes. In the long term, defect in autophagy clearance could contribute to neurodegeneration (Menzies et al., 2017). Accordingly, the accumulation of gangliosides in lysosomes paralleled the accumulation of p62 in lysosomes observed by Varga et al. (2015) and the progression of neurodegeneration that we observed in the *Spg11*$^{-/-}$ mice (Branchu et al., 2017). *In vitro*, glutamate treatment was proposed to inhibit the

(C) Quantification of neuronal death 30 hr after incubation of neurons with glutamate (200 μM) in primary cultures of *Spg11*$^{+/+}$ and *Spg11*$^{-/-}$ cortical neurons transfected with vectors that downregulate Neu1 with two independent miRNAs (Neu1-1 and Neu1-2). The graph shows the mean ± SEM values. N = 6 independent experiments. One-way ANOVA, followed by Holm-Sidak post hoc test; ***p < 0.001.

(D and E) Immunostaining (D) and quantification (E) of GM2 immunostaining in the telencephalon of morphants injected with 1.2-pmol *zspg11*^{spl} antisense or 1.2-pmol mismatch (mm) morpholino (MO). Injection of *zspg11*^{spl} morpholino increased the mean and variance of GM2 immunostaining intensity. This phenotype was corrected when morphants were treated with miglustat. N = 6–12 morphants analyzed in each condition. One-way ANOVA; ***p < 0.001.

(F) Phenotype of morphants that were non-injected or injected with 1.2-pmol *zspg11*^{spl} or 1.2-pmol mismatch (mm) morpholino. 48 hr post-fertilization, morphants were classified as normal phenotype, slowly swimming, paralyzed, or curly morphants. Injection of *zspg11*^{spl} morpholino leads a large proportion of paralyzed or slowly swimming phenotypes. Treatment with miglustat decreased the proportion of paralyzed morphants. N = 102–366 morphants analyzed in each groups. Chi square test; ***p < 0.0001.

(G and H) Tracking (G) and quantification of distance traveled (H) by larvae following a touch-evoked escape response. Injection of *zspg11*^{spl} morpholino impaired the swimming of morphants, which was corrected when treated by miglustat. The graph shows the mean ± SEM. N = 12 morphants analyzed in each condition. One-way ANOVA; ***p < 0.001.

See also Figure S6.

autophagic flux in hippocampal neurons leading to accumulation of p62 (Kulbe et al., 2014). Accordingly, decreasing ganglioside synthesis has a protective action against neuronal death induced by glutamate in *Spg11*$^{-/-}$ neurons, probably by preventing accumulation of the autophagy marker p62. Altogether, our results suggest that the accumulation of gangliosides and the subsequent accumulation of lysosomes containing autophagic markers are contributing to neuronal death in the absence of spatacsin.

Decreasing gangliosides synthesis therefore appears as a rational therapeutic strategy to prevent the symptoms caused by the accumulation of these glycosphingolipids in lysosomes. Consistently, diminution of gangliosides improved motor phenotype in an *in vivo* zebrafish model of SPG11. Such treatment should be started at very early stages of the disease as we showed early accumulation of gangliosides in lysosomes, both in the *Spg11* knockout mouse model and human SPG11 iPSC-derived neurons. However, it was not possible to test this hypothesis in the *Spg11*$^{-/-}$ mouse model due to the controversial action of miglustat on brain glycosphingolipids (Ashe et al., 2011; Boudewyn et al., 2017).

In conclusion, we show that gangliosides accumulate in lysosomes following impairment of lysosome membrane recycling, and not only upon metabolic impairment as observed in lysosomal storage disorders (Walkley and Vanier, 2009). The accumulation of gangliosides was responsible for accumulation of autophagy markers in lysosomes and neurodegeneration. Since gangliosides are highly present in the brain (Xu et al., 2010), our work reveals why proteins implicated in lysosome membrane recycling are often associated with neurodegeneration, and provides a rational therapeutic strategy for neurodegenerative diseases linked to such lysosomal dysfunction. Accumulation of undigested material in lysosomes with abnormal morphology was also observed in SPG4, SPG8, SPG15, SPG31, and SPG48 models of hereditary spastic paraplegias (Allison et al., 2017; Hirst et al., 2015; Renvoisé et al., 2014). It might be informative to investigate lysosome membrane recycling and ganglioside accumulation in these diseases. In addition, gangliosides accumulate in lysosomes in models of quite prevalent neurodegenerative diseases, such as Alzheimer's disease (Yang et al., 2014), and it would be interesting to test whether the recycling of lysosome membrane is altered in these conditions as well. This would allow a better understanding of the physiopathological pathway leading to neuronal death and indicate whether these patients can benefit from the same therapeutic approaches.

EXPERIMENTAL PROCEDURES

Ethical Approval

The care and treatment of animals followed European legislation (no. 2010/63/UE) and national (Ministère de l'Agriculture, France) guidelines for the detention, use, and ethical treatment of laboratory animals. All experiments on animals were approved by the local ethics committee (approval no. A751319 and ce5/2012/057) and conducted by authorized personnel. Patient-derived materials were obtained through procedures approved by the ethics committee with the written, informed consent of the family (approval RBM-1-029).

Spg11-Knockout Mouse Immunohistochemistry

Spg11-knockout mice were described previously (Branchu et al., 2017). Immunohistochemistry was performed as previously described (Branchu et al., 2017). Images were obtained with an Olympus FV-1000 confocal microscope with a 60× objective (numerical aperture [NA], 1.35). For quantification, regions of interest (ROIs) corresponding to the cell body of individual neurons were surrounded using ImageJ, and the mean of fluorescence intensity of ganglioside immunostaining in each ROI was quantified using the measure tool. In each brain slice, we analyzed all neurons that were identified by their morphology and large cell body in the layer V of the motor cortex.

Human SPG11 Fibroblasts

Skin biopsies were collected from two healthy female subjects and two SPG11 female patients. Patient SPG11-1 (FSP-1123-004) carried two heterozygous truncating mutations *in trans* (c.2431 C>T, pGln811X; deletion of exon 29). This patient had normal intellectual development and experienced gait difficulties by age 14, gradually worsened, and became stick-dependent at age 20. Examination at age 23 showed that she could still walk with sticks. Spasticity and weakness was present in the lower limbs, while tone and strength were normal in the upper limbs. She had increased reflexes with ankle clonus and bilateral extensor plantar reflex as well as Hoffman sign in the upper limbs. Deep sensation was normal. She had postural tremor in the arms, normal eye gaze, and no cognitive impairment. There was no evident cerebellar sign. Patient SPG11-2 (FSP-1232-003) carried two heterozygous truncating mutations *in trans* (c.1951 C>T, pArg651X; c.5623 C>T, pGln1875X). This woman had onset of spastic gait at age 17. At age 27, she presented with moderate spastic gait, needing walking aids since age 26, and more recently a wheelchair. She had increased reflexes in lower limbs, including bilateral extensor plantar reflexes, and Hoffman signs were present in the upper limbs. She had moderate weakness in the legs and decreased deep sensation at the ankles. Bradykinesia was evident, and the finger-nose test was performed with mild tremor. Cognition was clinically normal, and she exhibited no abnormal eye movements. Cerebral imaging showed a thin corpus callosum.

Zebrafish Modeling

Modeling of SPG11 pathology in zebrafish was performed using morpholino oligonucleotides as described previously (Martin et al., 2012). After morpholino injection, embryos were maintained at 28°C in E3 medium, containing miglustat or DMSO for control groups. At 24 hr post-fertilization (hpf), they were manually dechorionated using fine forceps. The embryo morphology was observed at 48 hr post-fertilization.

Biochemical Analyses

Experimental procedures for lipidomic analysis, lysosome fraction purification, and enzymatic assays are detailed in Supplemental Experimental Procedures.

Cell Culture

Experimental procedures for cultures of primary neurons and iPSCs, as well as differentiation of organoids are detailed in Supplemental Experimental Procedures.

Statistics

Statistics were performed using GraphPad Prism software, using the Kruskal-Wallis, ANOVA, or t tests, depending on the experiments. Multiple comparisons after ANOVA were performed with the Holm-Sidak test using GraphPad Prism. For lipidomic analysis, the mcp package was used with R, version 3.0.2. Comparison of the means between phenotypes was performed using a t test with a Benjamini-Hochberg procedure to correct for multiple testing, with a false-discovery rate of 5%.

SUPPLEMENTAL INFORMATION

Supplemental Information includes Supplemental Experimental Procedures, six figures, one table, and three videos and can be found with this article online at https://doi.org/10.1016/j.celrep.2018.05.098.

ACKNOWLEDGMENTS

We thank Phenoparc, Histomics, IGenSeq, Celis, Celis-IPS, and ICM.quant facilities of the Institut du Cerveau et de la Moelle Épinière for their contributions.

This work was supported by "Investissements d'Avenir" Program grants ANR-10-IAIHU-06 and ANR-11-INBS-0011 and received funding from the Verum Foundation (to A.B. and G.S.), the French Agency for Research (ANR) (13-ISV1-00002 to G.S. and MetaboHUB: ANR-11-INBS-0010), the GIS-Maladies Rares Foundation (06/GIS/PB/SJ/no.71 to G.S.), the Fondation Roger de Spoelberch (to A.B.), the European Union with the ANR (to A.B., Seventh Framework Programme–FP7, Omics Call [grant No. 305121]; to G.S., the E-Rare Programme Neurolipid [ANR-13-ERARE-0003-02]), and the European Research Council (European Research Council Starting Grant No. 311149 to F.D.). M.B. received a fellowship from the French Ministry of Research (Doctoral School ED3C). A.P. received an ARDoC fellowship (17012953) from the Région Ile de France (Doctoral School ED3C).

AUTHOR CONTRIBUTIONS

M.B., J.B., A.B., F.M., K.H.E.H., G.S., and F.D. conceived and designed the experiments. M.B., J.B., C.L., C.P., J.P., R.M., A.S., M.P., E.C.-V., A.P., K.D., J.-P.P., C.C., A.D., B.C., K.H.E.H., and F.D. performed the experiments. M.B., J.B., C.L., C.P., J.P., R.M., A.S., M.P., B.C., F.M., K.H.E.H., and F.D. analyzed the data. M.B., J.B., G.S., and F.D. wrote the paper.

DECLARATION OF INTERESTS

M.B., J.B., F.M., G.S., and F.D. have a patent related to this work.

Received: January 24, 2018
Revised: April 24, 2018
Accepted: May 30, 2018
Published: June 26, 2018

REFERENCES

Allison, R., Edgar, J.R., Pearson, G., Rizo, T., Newton, T., Günther, S., Berner, F., Hague, J., Connell, J.W., Winkler, J., et al. (2017). Defects in ER-endosome contacts impact lysosome function in hereditary spastic paraplegia. J. Cell Biol. *216*, 1337–1355.

Ashe, K.M., Bangari, D., Li, L., Cabrera-Salazar, M.A., Bercury, S.D., Nietupski, J.B., Cooper, C.G., Aerts, J.M., Lee, E.R., Copeland, D.P., et al. (2011). Iminosugar-based inhibitors of glucosylceramide synthase increase brain glycosphingolipids and survival in a mouse model of Sandhoff disease. PLoS One *6*, e21758.

Bonten, E., van der Spoel, A., Fornerod, M., Grosveld, G., and d'Azzo, A. (1996). Characterization of human lysosomal neuraminidase defines the molecular basis of the metabolic storage disorder sialidosis. Genes Dev. *10*, 3156–3169.

Boudewyn, L.C., Sikora, J., Kuchar, L., Ledvinova, J., Grishchuk, Y., Wang, S.L., Dobrenis, K., and Walkley, S.U. (2017). N-Butyldeoxynojirimycin delays motor deficits, cerebellar microgliosis, and Purkinje cell loss in a mouse model of mucolipidosis type IV. Neurobiol. Dis. *105*, 257–270.

Branchu, J., Boutry, M., Sourd, L., Depp, M., Leone, C., Corriger, A., Vallucci, M., Esteves, T., Matusiak, R., Dumont, M., et al. (2017). Loss of spatacsin function alters lysosomal lipid clearance leading to upper and lower motor neuron degeneration. Neurobiol. Dis. *102*, 21–37.

Chang, J., Lee, S., and Blackstone, C. (2014). Spastic paraplegia proteins spastizin and spatacsin mediate autophagic lysosome reformation. J. Clin. Invest. *124*, 5249–5262.

Du, W., Su, Q.P., Chen, Y., Zhu, Y., Jiang, D., Rong, Y., Zhang, S., Zhang, Y., Ren, H., Zhang, C., et al. (2016). Kinesin 1 drives autolysosome tubulation. Dev. Cell *37*, 326–336.

Folch, J., Lees, M., and Sloane Stanley, G.H. (1957). A simple method for the isolation and purification of total lipides from animal tissues. J. Biol. Chem. *226*, 497–509.

Hehr, U., Bauer, P., Winner, B., Schule, R., Olmez, A., Koehler, W., Uyanik, G., Engel, A., Lenz, D., Seibel, A., et al. (2007). Long-term course and mutational spectrum of spatacsin-linked spastic paraplegia. Ann. Neurol. *62*, 656–665.

Hirst, J., Edgar, J.R., Esteves, T., Darios, F., Madeo, M., Chang, J., Roda, R.H., Durr, A., Anheim, M., Gellera, C., et al. (2015). Loss of AP-5 results in accumulation of aberrant endolysosomes, defining a new type of lysosomal storage disease. Hum. Mol. Genet. *24*, 4984–4996.

Jeyakumar, M., Butters, T.D., Cortina-Borja, M., Hunnam, V., Proia, R.L., Perry, V.H., Dwek, R.A., and Platt, F.M. (1999). Delayed symptom onset and increased life expectancy in Sandhoff disease mice treated with N-butyldeoxynojirimycin. Proc. Natl. Acad. Sci. USA *96*, 6388–6393.

Kanagaraj, P., Gautier-Stein, A., Riedel, D., Schomburg, C., Cerdà, J., Vollack, N., and Dosch, R. (2014). Souffle/Spastizin controls secretory vesicle maturation during zebrafish oogenesis. PLoS Genet. *10*, e1004449.

Kulbe, J.R., Mulcahy Levy, J.M., Coultrap, S.J., Thorburn, A., and Bayer, K.U. (2014). Excitotoxic glutamate insults block autophagic flux in hippocampal neurons. Brain Res. *1542*, 12–19.

Lewerenz, J., and Maher, P. (2015). Chronic glutamate toxicity in neurodegenerative diseases—what is the evidence? Front. Neurosci. *9*, 469.

Martin, E., Yanicostas, C., Rastetter, A., Alavi Naini, S.M., Maouedj, A., Kabashi, E., Rivaud-Péchoux, S., Brice, A., Stevanin, G., and Soussi-Yanicostas, N. (2012). Spatacsin and spastizin act in the same pathway required for proper spinal motor neuron axon outgrowth in zebrafish. Neurobiol. Dis. *48*, 299–308.

Menzies, F.M., Fleming, A., Caricasole, A., Bento, C.F., Andrews, S.P., Ashkenazi, A., Füllgrabe, J., Jackson, A., Jimenez Sanchez, M., Karabiyik, C., et al. (2017). Autophagy and neurodegeneration: pathogenic mechanisms and therapeutic opportunities. Neuron *93*, 1015–1034.

Mizushima, N., Yamamoto, A., Matsui, M., Yoshimori, T., and Ohsumi, Y. (2004). In vivo analysis of autophagy in response to nutrient starvation using transgenic mice expressing a fluorescent autophagosome marker. Mol. Biol. Cell *15*, 1101–1111.

Nakano, Y., Fujitani, K., Kurihara, J., Ragan, J., Usui-Aoki, K., Shimoda, L., Lukacsovich, T., Suzuki, K., Sezaki, M., Sano, Y., et al. (2001). Mutations in the novel membrane protein spinster interfere with programmed cell death and cause neural degeneration in *Drosophila melanogaster*. Mol. Cell. Biol. *21*, 3775–3788.

Park, D.H., Wang, L., Pittock, P., Lajoie, G., and Whitehead, S.N. (2016). Increased expression of GM1 detected by electrospray mass spectrometry in rat primary embryonic cortical neurons exposed to glutamate toxicity. Anal. Chem. *88*, 7844–7852.

Paşca, A.M., Sloan, S.A., Clarke, L.E., Tian, Y., Makinson, C.D., Huber, N., Kim, C.H., Park, J.Y., O'Rourke, N.A., Nguyen, K.D., et al. (2015). Functional cortical neurons and astrocytes from human pluripotent stem cells in 3D culture. Nat. Methods *12*, 671–678.

Renvoisé, B., Chang, J., Singh, R., Yonekawa, S., FitzGibbon, E.J., Mankodi, A., Vanderver, A., Schindler, A., Toro, C., Gahl, W.A., et al. (2014). Lysosomal abnormalities in hereditary spastic paraplegia types SPG15 and SPG11. Ann. Clin. Transl. Neurol. *1*, 379–389.

Rong, Y., McPhee, C.K., Deng, S., Huang, L., Chen, L., Liu, M., Tracy, K., Baehrecke, E.H., Yu, L., and Lenardo, M.J. (2011). Spinster is required for autophagic lysosome reformation and mTOR reactivation following starvation. Proc. Natl. Acad. Sci. USA *108*, 7826–7831.

Rong, Y., Liu, M., Ma, L., Du, W., Zhang, H., Tian, Y., Cao, Z., Li, Y., Ren, H., Zhang, C., et al. (2012). Clathrin and phosphatidylinositol-4,5-bisphosphate regulate autophagic lysosome reformation. Nat. Cell Biol. *14*, 924–934.

Schulze, R.J., Weller, S.G., Schroeder, B., Krueger, E.W., Chi, S., Casey, C.A., and McNiven, M.A. (2013). Lipid droplet breakdown requires dynamin 2 for vesiculation of autolysosomal tubules in hepatocytes. J. Cell Biol. *203*, 315–326.

Sridhar, S., Patel, B., Aphkhazava, D., Macian, F., Santambrogio, L., Shields, D., and Cuervo, A.M. (2013). The lipid kinase PI4KIIIβ preserves lysosomal identity. EMBO J. *32*, 324–339.

Stevanin, G., Santorelli, F.M., Azzedine, H., Coutinho, P., Chomilier, J., Denora, P.S., Martin, E., Ouvrard-Hernandez, A.M., Tessa, A., Bouslam, N., et al. (2007). Mutations in SPG11, encoding spatacsin, are a major cause of spastic paraplegia with thin corpus callosum. Nat. Genet. *39*, 366–372.

Tesson, C., Koht, J., and Stevanin, G. (2015). Delving into the complexity of hereditary spastic paraplegias: how unexpected phenotypes and inheritance modes are revolutionizing their nosology. Hum. Genet. *134*, 511–538.

Tettamanti, G., Bassi, R., Viani, P., and Riboni, L. (2003). Salvage pathways in glycosphingolipid metabolism. Biochimie *85*, 423–437.

Varga, R.E., Khundadze, M., Damme, M., Nietzsche, S., Hoffmann, B., Stauber, T., Koch, N., Hennings, J.C., Franzka, P., Huebner, A.K., et al. (2015). In vivo evidence for lysosome depletion and impaired autophagic clearance in hereditary spastic paraplegia type SPG11. PLoS Genet. *11*, e1005454.

Walkley, S.U., and Vanier, M.T. (2009). Secondary lipid accumulation in lysosomal disease. Biochim. Biophys. Acta *1793*, 726–736.

Xu, Y.H., Barnes, S., Sun, Y., and Grabowski, G.A. (2010). Multi-system disorders of glycosphingolipid and ganglioside metabolism. J. Lipid Res. *51*, 1643–1675.

Yang, D.S., Stavrides, P., Saito, M., Kumar, A., Rodriguez-Navarro, J.A., Pawlik, M., Huo, C., Walkley, S.U., Saito, M., Cuervo, A.M., and Nixon, R.A. (2014). Defective macroautophagic turnover of brain lipids in the TgCRND8 Alzheimer mouse model: prevention by correcting lysosomal proteolytic deficits. Brain *137*, 3300–3318.

Yu, L., McPhee, C.K., Zheng, L., Mardones, G.A., Rong, Y., Peng, J., Mi, N., Zhao, Y., Liu, Z., Wan, F., et al. (2010). Termination of autophagy and reformation of lysosomes regulated by mTOR. Nature *465*, 942–946.

Cell Reports, Volume *23*

Supplemental Information

Inhibition of Lysosome Membrane Recycling Causes Accumulation of Gangliosides that Contribute to Neurodegeneration

Maxime Boutry, Julien Branchu, Céline Lustremant, Claire Pujol, Julie Pernelle, Raphaël Matusiak, Alexandre Seyer, Marion Poirel, Emeline Chu-Van, Alexandre Pierga, Kostantin Dobrenis, Jean-Philippe Puech, Catherine Caillaud, Alexandra Durr, Alexis Brice, Benoit Colsch, Fanny Mochel, Khalid Hamid El Hachimi, Giovanni Stevanin, and Frédéric Darios

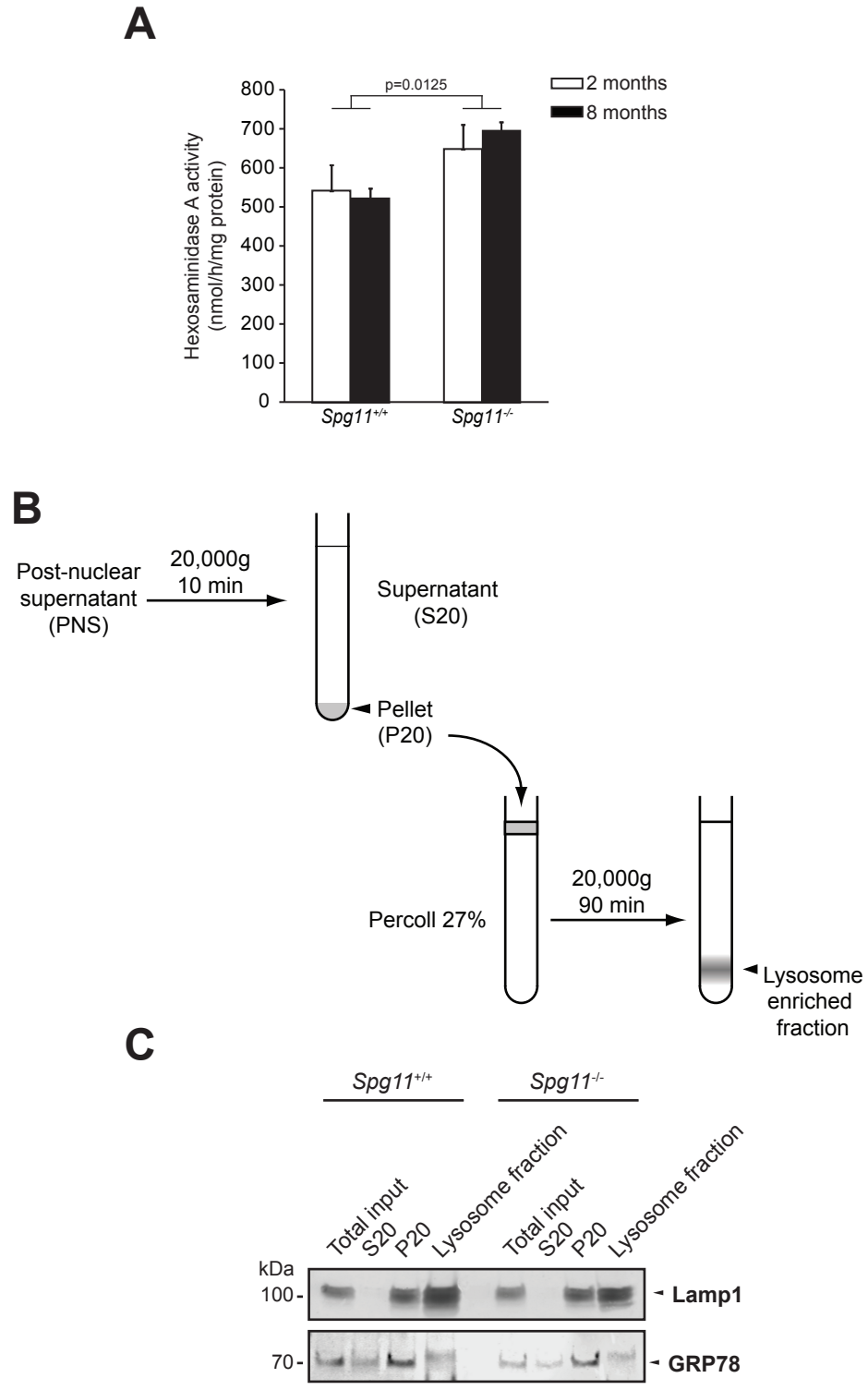

Figure S1: Investigation of lysosome functions in *Spg11*$^{+/+}$ and *Spg11*$^{-/-}$ mouse brain.
Related to Figure 1 and Table 1.
(**A**) Hexosaminidase A activity monitored in cortex of *Spg11*$^{+/+}$ and *Spg11*$^{-/-}$ mice. N=5. Two-way ANOVA. (**B**) Scheme showing the procedure used to purify fractions enriched in lysosomes. (**C**) Western blot analysis of whole brain lysate, fractions S20, P20, and the lysosome-enriched fraction obtained from *Spg11*$^{+/+}$ and *Spg11*$^{-/-}$ mouse brain.

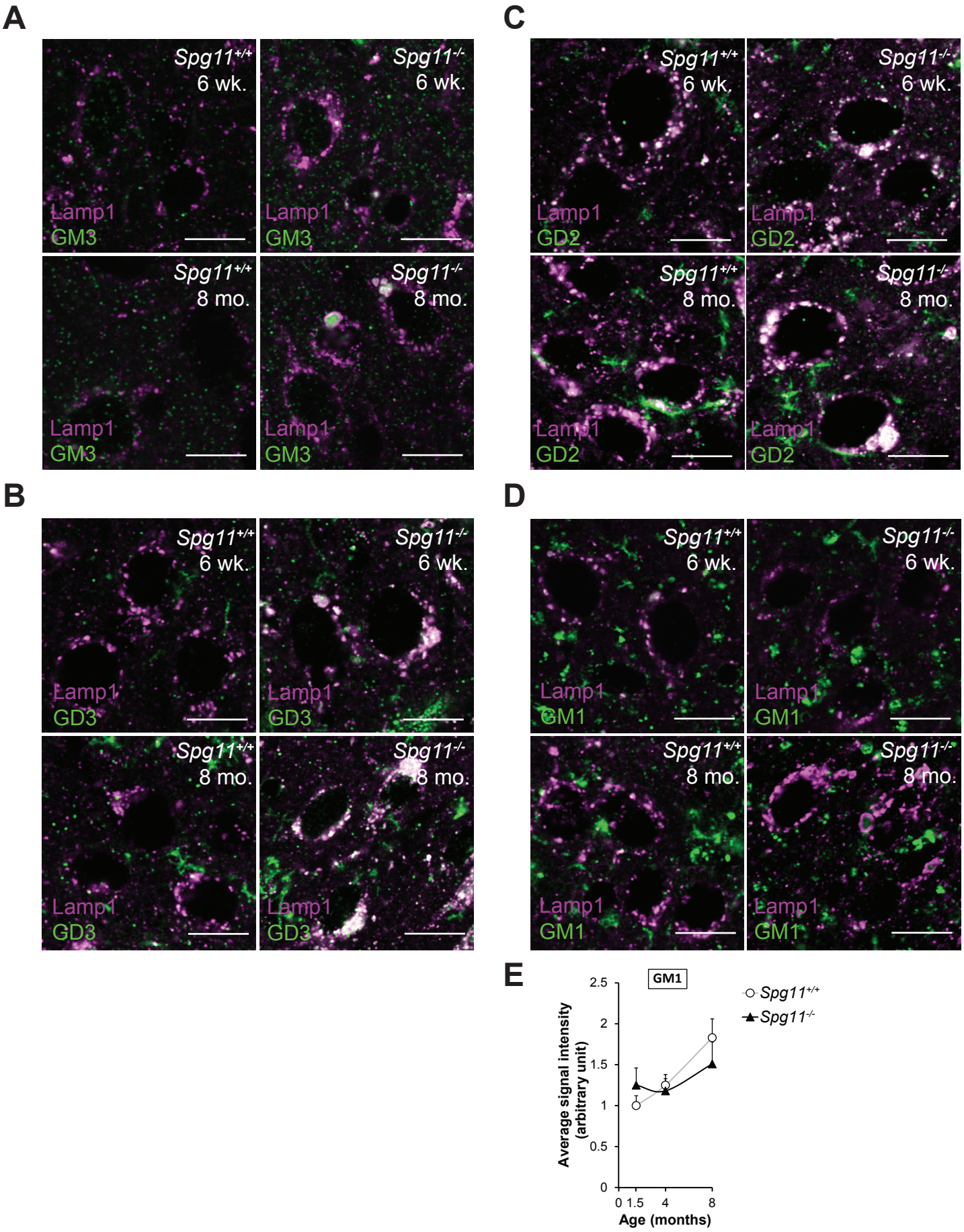

Figure S2. Spatacsin loss promotes lysosomal accumulation of gangliosides in neurons of the cortex. Related to Figure 1.

(**A-D**) Immunostaining of Lamp1 (magenta) and GM3 (**A**), GD3 (**B**), GD2 (**C**) and GM1 (**D**) in Spg11$^{+/+}$ and Spg11$^{-/-}$ cortical motor neurons of the layer V of the motor cortex from six-week-old (6wk.) and eight-month-old (8 mo.) mice. Scale bars: 10 µm. (**E**) Quantification of the mean of the GM1 immunostaining intensity per neuron. Quantification was performed in neurons of the layer V of motor cortex that were detected by their large soma. The graph shows the mean ± SEM values. N = 10-15 neurons quantified in five cortex slices of 5 five independent mice.

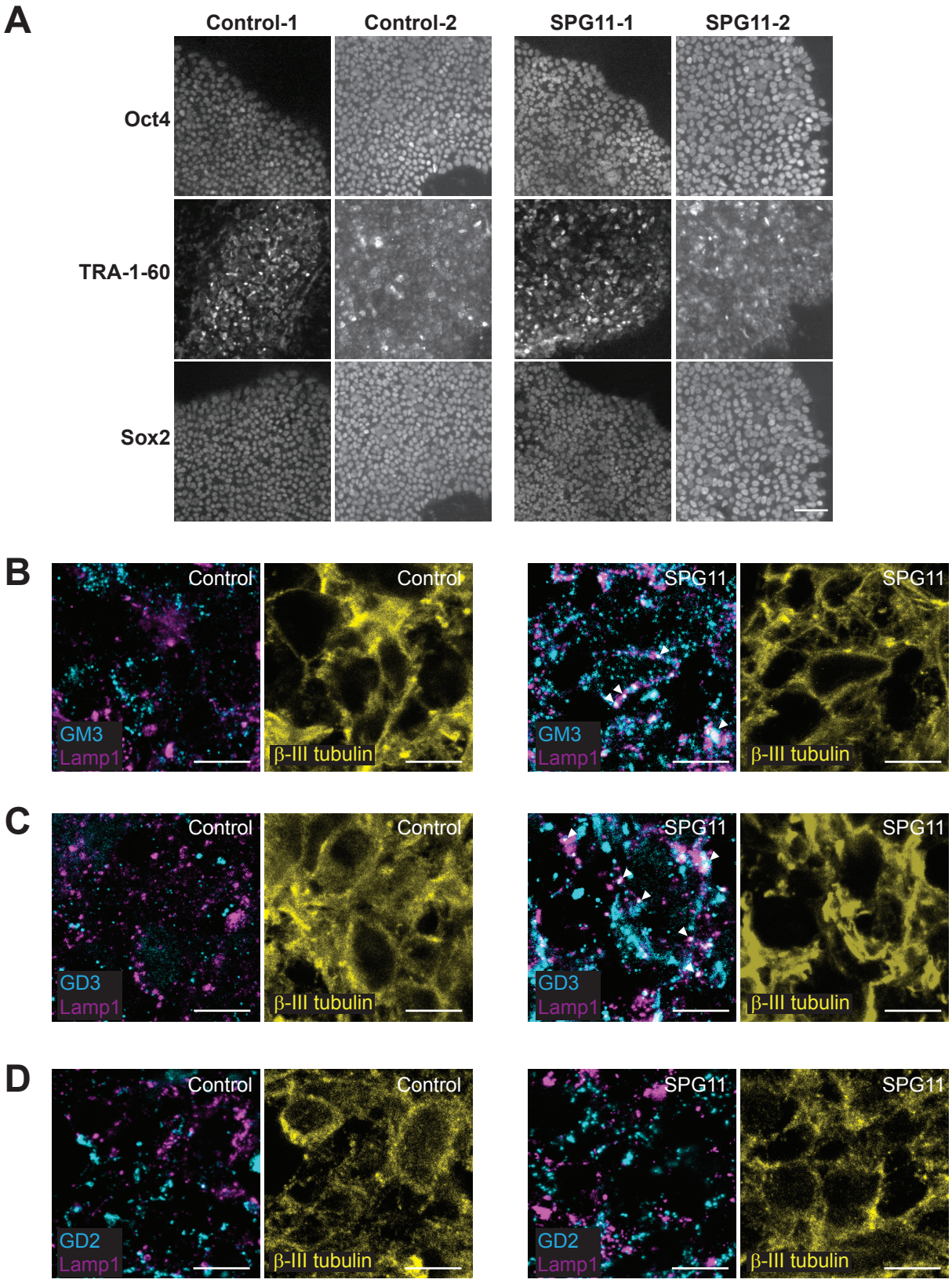

Figure S3. Spatacsin loss promotes lysosomal accumulation of GM3 and GD3 gangliosides in neurons derived from SPG11 patients. Related to Figure 2.

(**A**) Immunostaining of iPS cells with pluripotency markers. Scale bar: 20µm.

(**B-D**) Immunostaing of Lamp1 (magenta) and GM3 (B), GD3 (C) or GD2 (D) in the neuronal layer of organoids derived from healthy subjects (Control) or SPG11 patients. βIII-tubulin (yellow) shows the neuronal identity of the cells that were analyzed. Confocal microscopy images showing the accumulation of GM3- and GD3-positive staining in lysosomes labelled by Lamp1 staining of organoids derived from SPG11 patients (arrowheads). Scale bars: 10 µm.

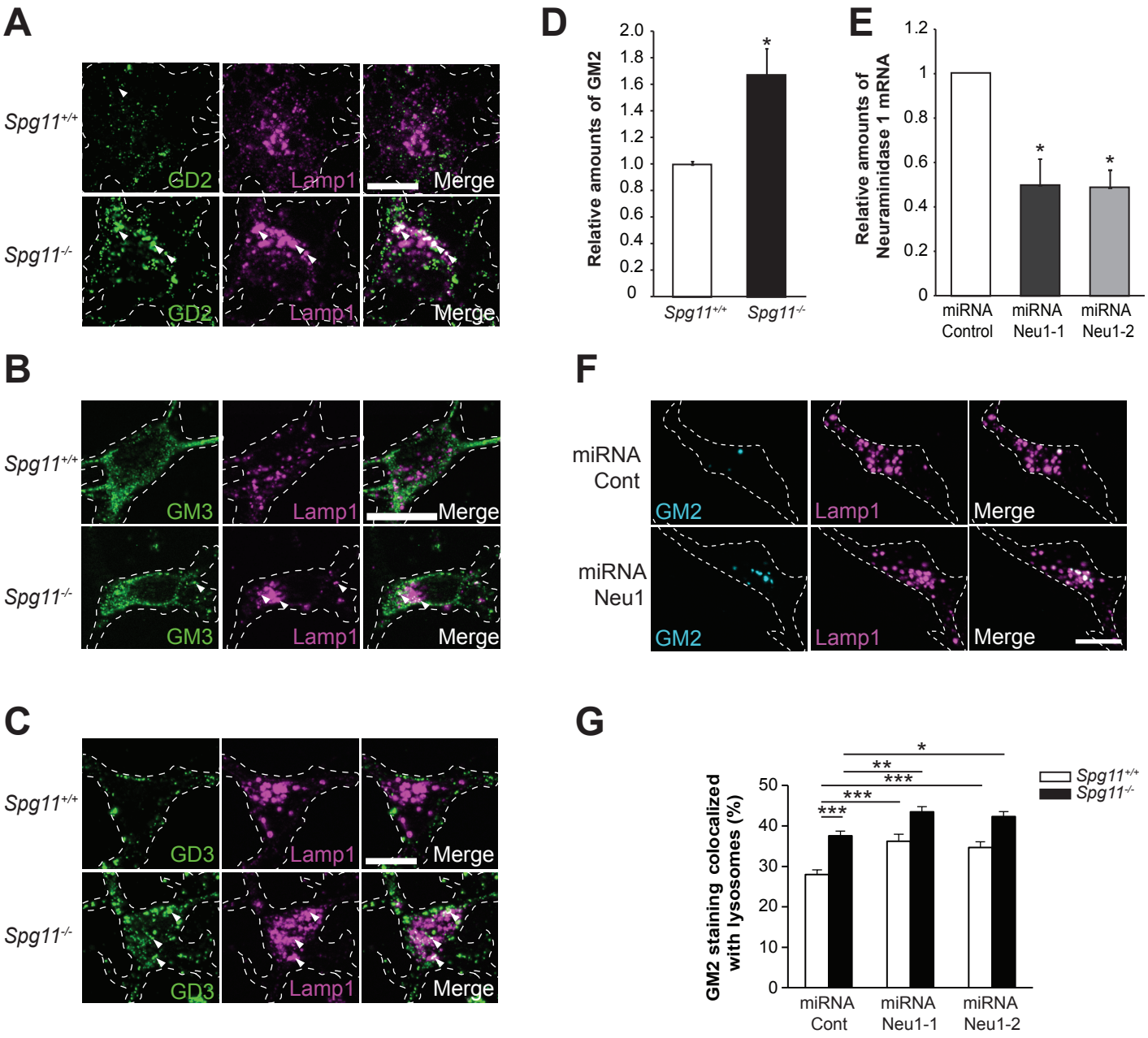

Figure S4: Downregulation of Neu1 increases ganglioside levels in lysosomes in cultured wild-type neurons. Related to Figure 3

(**A-C**) Immunostaining of Lamp1 (magenta) and GD2 (**A**), GM3 (**B**) and GD3 (**C**) in *Spg11*$^{+/+}$ and *Spg11*$^{-/-}$ neurons cultured for six days *in vitro*. Confocal microscopy images showing the accumulation of gangliosides in lysosomes labeled by Lamp1 staining. Scale bars: 10 µm. (**D**) Relative amount of GM2 monitored by lipidomic analysis in *Spg11*$^{+/+}$ and *Spg11*$^{-/-}$ neurons cultured for six days *in vitro*. N = 5 and 6 neuronal preparations for *Spg11*$^{+/+}$ and *Spg11*$^{-/-}$ neurons, respectively. Welsh's t-test, p=0.026. (**E**) qRT-PCR showing the decrease in Neu1 mRNA in mouse NIH-3T3 cells transfected with the vectors expressing two different miRNAs targeting Neu1 or a control vector. N = 4. Kruskal-Wallis test, *p < 0.05. (**F**) Effect of Neu1 downregulation on staining with antibodies directed against GM2 (cyan) and Lamp1 (magenta). Note the increase in the number of lysosomes labeled with GM2 after downregulation of Neu1. Scale bar: 10 µm. (**G**) Quantification of the proportion of GM2 staining that is localized to lysosomes in neurons transfected with vectors expressing two independent miRNAs directed against Neu1. The graph shows the mean ± SEM values. N = 49-61 neurons quantified in three independent neuron preparations. Two-way ANOVA, followed by Holm-Sidak post-hoc test; *p < 0.05; **p < 0.01; ***p < 0.001.

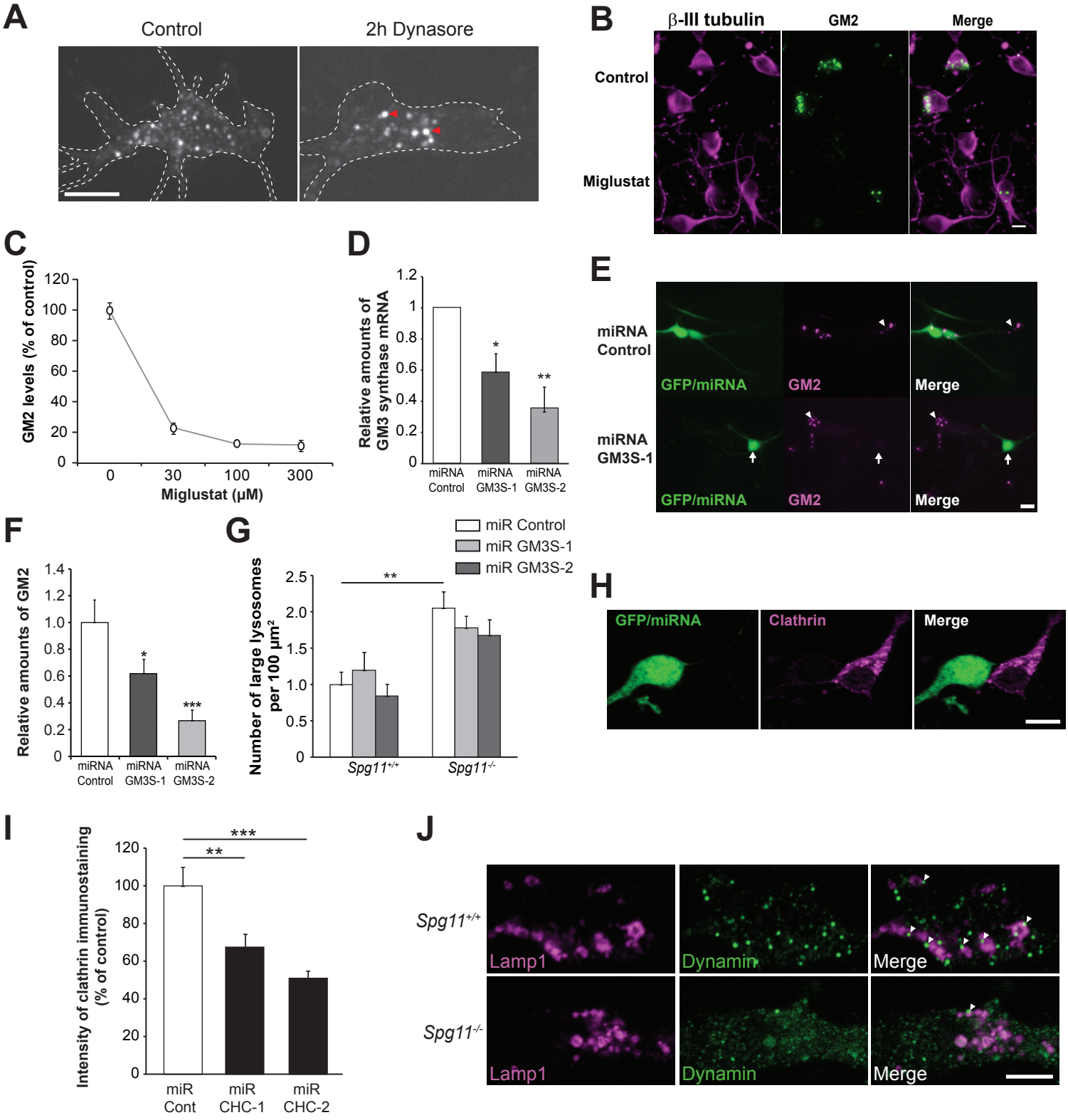

Figure S5. Inhibition of ganglioside synthesis decreases ganglioside levels in cultured neurons. Related to Figure 4.
(**A**) Iive imaging of neurons expressing Lamp1-mcherry, treated with vehicle or Dynasore (40μM) for 2 hours. Arrowheads point to lysosomes with a diameter larger than 1μm. Scale bar: 10μm. **(B)** β–III tubulin (magenta, neuronal marker) and GM2 immunostaining (green) of primary cultures of cortical neurons treated or not with miglustat (100μM) for six days *in vitro*. Scale bar: 10μm. **(C)** Quantification of the fluorescence intensity of GM2 immunostaining of primary cultures of cortical neurons cultured for six days *in vitro* with various concentrations of miglustat. The graph shows the mean ± SEM values. N = 3 independent experiments. **(D)** qRT-PCR showing the decrease in GM3 synthase mRNA in mouse NIH-3T3 cells transfected with the vectors expressing two different miRNAs targeting the GM3 synthase or a control vector. N = 3. Kruskal-Wallis test, *p = 0.048; **p=0.003. **(E)** GM2 immunostaining (magenta) of cells transfected with vector expressing GFP and miRNA to downregulate GM3 synthase. The arrow indicates a cell transfected with miRNA against GM3 synthase, showing weak GM2 immunostaining. Arrowheads indicate non-transfected cells. Scale bar: 10μm. **(F)** Quantification of the fluorescence intensity of GM2 in neurons transfected with vectors

expressing control miRNA or two different miRNA against GM3 synthase. N = 45-63 neurons in two independent experiments. One-way ANOVA, followed by Holm-Sidak post-hoc test; *p=0.03, ***p<0.001. **(G)** Quantification of the number of lysosomes with a diameter larger than 1µm in *Spg11*$^{+/+}$ and *Spg11*$^{-/-}$ neurons expressing control miRNA or miRNA downregulating GM3 synthase. The graph shows the mean ± SEM values. N = 14-33 neurons quantified in three independent neuron preparations. One-way ANOVA, followed by Holm-Sidak post-hoc test; **p=0.0024. **(H)** Clathrin heavy chain immunostaining of neurons transfected with vector expressing GFP and miRNA to downregulate clathrin heavy chain. **(I)** Quantificationof the intensity of clathrin immunostaining in neurons transfected with vectors expressing control miRNA or miRNA downregulating clathrin heavy chain. The graph shows the mean ± SEM values. N =44-53 neurons quantified in two independent neuron preparations. One-way ANOVA, followed by Holm-Sidak post-hoc test; **p=0.0016, ***p<0.001. **(J)** Lamp1 (magenta) and dynamin (green) immunostaining of *Spg11*$^{+/+}$ and *Spg11*$^{-/-}$ neurons showing decreased recruitment of dynamin to lysosomes in *Spg11*$^{-/-}$ neurons. Arrowheads point recruitment of dynamin at the edge of lysosomes. Scale bar: 5µm.

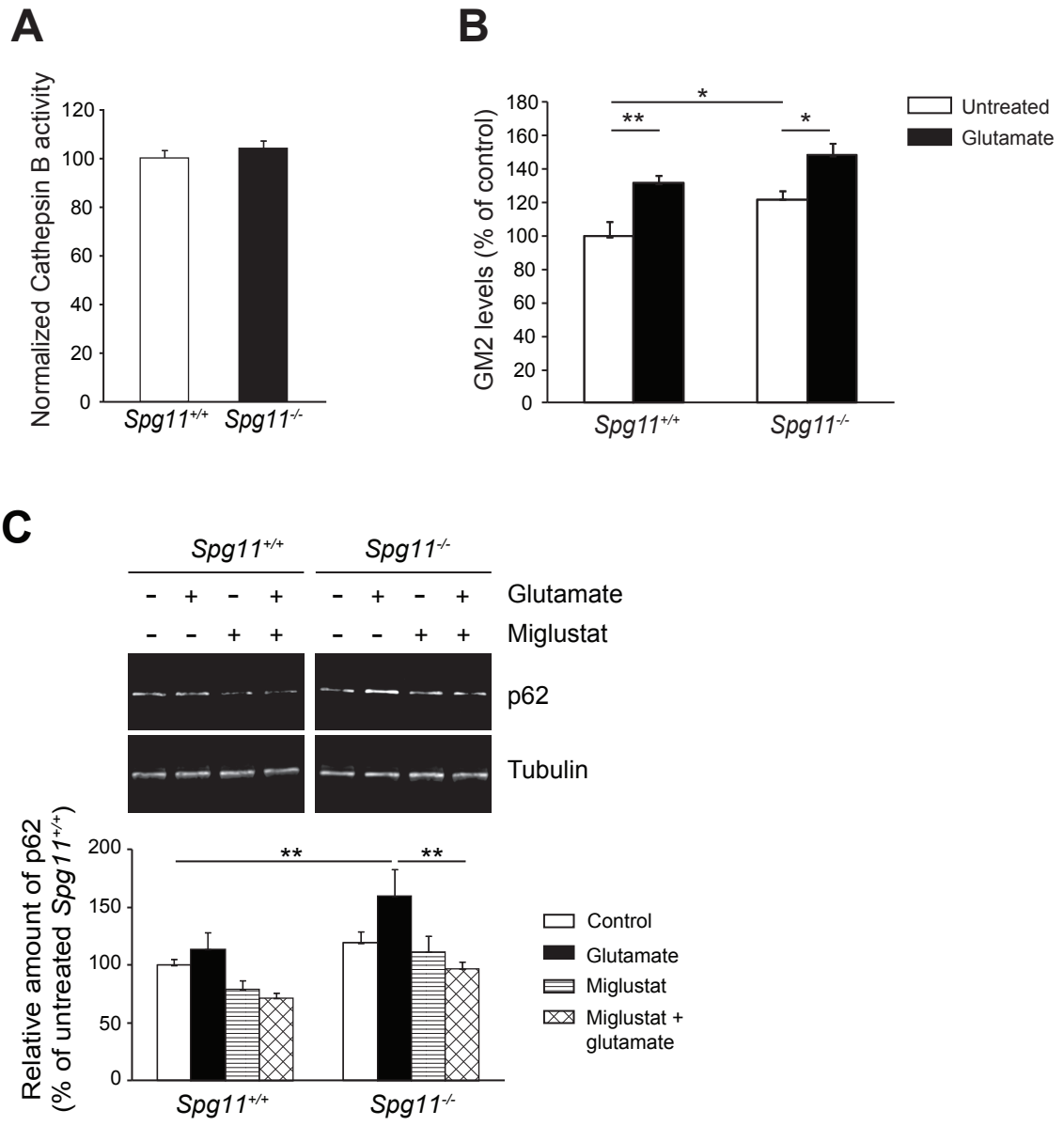

Figure S6: Glutamate treatment increases GM2 levels in *Spg11*$^{+/+}$ and *Spg11*$^{-/-}$ neurons.
Related to Figure 5.

(**A**) Normalized catalytic activity of cathepsin B monitored with the Magic Red Cathepsin B Assay Kit in primary cultures of *Spg11*$^{+/+}$ and *Spg11*$^{-/-}$ neurons after six days in vitro. N = 3 independent experiments performed in quadruplicate. (**B**) Quantification of fluorescence intensity of GM2 immunostaining of primary cultures of *Spg11*$^{+/+}$ and *Spg11*$^{-/-}$ cortical neurons that were treated for 24 hours with 200µM glutamate. The graph shows the mean ± SEM values. N = 7-10 independent neuron preparations. One-way ANOVA, followed by Holm-Sidak post-hoc test;* $p<0.05$, ** $p<0.01$. (**C**) Western blot analysis of p62 levels in *Spg11*$^{+/+}$ and *Spg11*$^{-/-}$ cortical neurons treated or not with miglustat (100 µM). Neurons were incubated with glutamate (200 µM) for 24 hours. Graph showing the quantification of the relative amount of p62 normalized to tubulin in *Spg11*$^{+/+}$ and *Spg11*$^{-/-}$ cortical neurons treated with miglustat or glutamate. N = 5-9 independent experiments. One-way ANOVA, followed by Holm-Sidak post-hoc test; **$p < 0.01$.

	Spg11$^{+/+}$	*Spg11*$^{-/-}$	Fold change
Fatty Acyls	**N=8**	**N=8**	
Total Free fatty acids (FA)	**87.31 ± 5.12**	**61.74 ± 4.54***	**0.71**
Glycerolipids			
Total Diacylglycerols (DG)	25.44 ± 2.31	23.68 ± 2.04	0.93
Total Triacylglycerols (TG)	39.92 ± 3.79	33.13 ± 4.22	0.83
Total Cardiolipines (CL)	11.01 ± 0.92	10.39 ± 0.61	0.94
Glycerophospholipids			
Total Lyso-Glycerophosphocholines (LPC)	**60.62 ± 4.32**	**43.46 ± 3.02***	**0.72**
Total Lyso-Glycerophosphoethanolamines (LPE)	**4.96 ± 0.36**	**3.66 ± 0.23***	**0.74**
Total Lyso-Glycerophosphoinositols (LPI)	**5.40 ± 0.28**	**3.51 ± 0.36***	**0.65**
Total Lyso-Glycerophosphoserines (LPS)	**5.31 ± 0.27**	**3.54 ± 0.30***	**0.67**
Total Glycerophosphocholines (PC)	15685.80 ± 1134.25	14329.06 ± 819.96	0.91
Total Glycerophosphoethanolamines (PE)	2668.36 ± 124.22	2491.88 ± 80.92	0.93
Total Glycerophosphoglycerols (PG)	38.18 ± 2.32	36.38 ± 1.38	0.95
Total Glycerophosphoinositols (PI)	603.44 ± 25.71	552.21 ± 23.50	0.92
Total Glycerophosphoserines (PS)	512.32 ± 26.65	472.93 ± 35.49	0.92
Sphingolipids			
Total Ceramides	**55.41 ± 5.44**	**37.66 ± 1.98***	**0.68**
Total Hexosylceramides	67.68 ± 7.19	60.37 ± 8.78	0.89
Total Gangliosides GM1	13.34 ± 1.08	10.68 ± 0.82	0.80
Total Gangliosides GM2	**0.39 ± 0.04**	**0.58 ± 0.05***	**1.49**
Total Gangliosides GM3	1.05 ± 0.09	1.11 ± 0.08	1.06
Total Gangliosides GD1	76.04 ± 4.83	61.41 ± 3.27	0.81
Total Sphingomyelins	548.17 ± 35.66	541.73 ± 23.91	0.99
Total Sulfoglycosphingolipids	576.35 ± 57.57	501.79 ± 65.14	0.87
Sterol Lipids			
Total Steryl esters	0.86 ± 0.10	0.79 ± 0.08	0.92
Cholesterol	61.61 ± 2.04	58.08 ± 1.82	0.94

Table S1: Relative amounts of various classes of lipids in the cortex of eight-month-old *Spg11*$^{+/+}$ and *Spg11*$^{-/-}$ mice. Related to Figure 1

Arbitrary units, normalized to tissue weight.*$p < 0.05$, T-test with Benjamini-Hochberg procedure to correct for multiple testing. Significant differences are highlighted in bold.

Supplemental Experimental Procedures

Antibodies and Chemicals

Miglustat was obtained from Tocris and dynasore was purchased from Abcam. Antibodies used in the study were: rat anti-Lamp1 (Clone 1D4B, Development Study Hybridoma Bank, University of Iowa), mouse anti-Lamp1 (clone H5G11; Santa Cruz Biotechnologies), mouse anti-GRP78 (BD Biosciences), mouse anti-p62 (Abcam), mouse-anti-clathrin (clone X-22, Abcam for immunocytochemistry; clone 23, BD Biosciences for western blotting), rabbit anti-Pax-6 (Covance), mouse anti-βIII-tubulin (Tuj1; Eurogentec), rabbit anti-sox2 (Millipore), mouse anti-oct4 (Santa Cruz biotechnology), mouse anti-Tra1-60 (Millipore), mouse anti-GM2 (hybridoma supernatant produced in-house) (Dobrenis et al., 1992; Natoli et al., 1986), mouse anti-GM3 (Cosmo Bio), mouse anti-GD2 (Millipore), and mouse anti-GD3 (Invitrogen), rabbit anti-dynamin1 (Abcam), mouse anti-dynamin (BD biosciences). For immunoblotting, the secondary antibodies were conjugated to either fluorochromes (IR-dye 800 or IR-dye 680; LI-COR) for detection with the Odyssey CLX infrared imaging system (Licor), or to horseradish peroxidase (Jackson Immunoresearch) for detection with the Supersignal West Pico Chemiluminescent Substrate (Pierce). Secondary antibodies used for immunofluorescence were purchased from Life Technologies.

Lipidomic analysis

Eight month-old *Spg11*$^{-/-}$ and *Spg11*$^{+/+}$ mice were killed by CO_2 and the cerebral cortices were immediately dissected and frozen in isopentane. Samples were extracted according to a modified Folch method (Folch et al., 1957). Briefly, 10 mg of cortex was added to 190 µL of chloroform/methanol 2:1 (v/v). Samples were vortexed for 60 s and then sonicated for 30 s using a sonication probe. Extraction was performed after 2 h at 4°C with mixing. In addition, 40 µL of ultra-pure water was added and samples were vortexed for 60 s before centrifugation at 10 000 rpm for 10 min at 4°C. The upper phase (aqueous phase), containing ganglioside species and several lysophospholipids, was transferred into a glass tube and then dried under a stream of nitrogen. The interphase which consists on a protein disk was discarded and the lower rich-lipid phase (organic phase) was pooled with the dried upper phase. Samples were then reconstituted with 200 µL of chloroform/methanol 2:1 (v/v), vortexed for 30 s, sonicated for 60 s, and diluted 1/100 in MeOH/IPA/H2O 65:35:5 (v/v/v) before injection.

All samples were processed and analyzed as described previously (Seyer et al., 2016). After liquid chromatography-high-resolution mass spectrometry analysis, samples were re-injected for higher energy collisional dissociation (HCD) tandem mass spectrometry experiments (MS/MS) in the negative ion mode, with the instrument set in the targeted mode, using inclusion lists. The isolation width was set to *m/z* 0.4, the normalized collision energy was 26%, and mass resolution was set to 17,500 FWHM at *m/z* 200. HCD mass spectra were inspected manually to confirm the identity of the ganglioside species. The relative amount of each lipid was quantified as the area of its chromatographic peak, and it was normalized to the exact weight of each cortex to take into account the difference of weight between cortices of *Spg11*$^{-/-}$ and *Spg11*$^{+/+}$ neurons.

Lysosome fractions

Lysosome-enriched fractions were purified from whole brains of eight-month old animals following the self-generated Percoll gradient protocol described previously (Graham, 2001) (Fig S1). At the end of the protocol, the lysosome-enriched fractions were washed once in PBS and the protein quantified by the BCA kit (Pierce). Western blots were performed as described previously (Esteves et al., 2014). Quantifications of band intensities on western blot was performed with the Gels plugin in Image J. Lysosome-enriched fractions were extracted according to the Folch procedure (Folch et al., 1957). The desalted Folch upper phases (aqueous phases), containing gangliosides, were analyzed by liquid chromatography coupled with high resolution mass spectrometry (LC-HRMS) in the negative ionization mode to detect deprotonated singly [M-H]- and doubly charged ions [M-2H]2-. Data were treated and analyzed as described previously (Seyer et al., 2016). The relative amount of each lipid was quantified as the area of its chromatographic peak, and it was normalized to the concentration of proteins in each lysosome-enriched fraction.

Hexosaminidase A activity

Hexosaminidase A activity was monitored as previously described (Niemir et al., 2018). Fifty mg of cortex were ground in 300 µl of 0.1 M citrate phosphate buffer, pH 4.5 and homogenates were lysed by three cycles of rapid freezing and thawing, followed by centrifugation at 4°C for 5 min at 10 000 g. The protein content of each supernatant was determined using the BCA kit. In a black 96-well plate with clear bottom, 10 µl of 1/10-diluted supernatant was added to 50 µl of the fluorimetric β-hexosaminidase A substrate [4-methylumbelliferyl-7–(6-sulfo-2-acetamido-2-deoxy-β-D-glucopyranoside (Calbiochem) at 1 mM in 0.1 M citrate phosphate buffer at pH 4.5]. The samples were incubated for 1 h at 37°C with gentle agitation and enzymatic reactions were stopped by adding 200 µl of a 1M glycine buffer, pH 10. The released fluorescence was read on a CytoFluor 4000 fluorimeter (PerSeptive Biosystems), excitation: 360 ± 40 nm, emission: 460 ± 40 nm. The data obtained were compared with the fluorescence of a 4-methyl-umbelliferone standard (10 nmol/well). Enzyme activity was expressed as nmol/h/mg cell protein.

Cellular reprogramming, characterization, and differentiation of iPS cells

Fibroblasts were reprogrammed into iPS cells by transient expression of OCT3/4, L-MYC, SOX2, KLF4, and LYN28 using episomal vectors as previously described (Okita et al., 2011). iPS cells were cultured on Geltrex matrix in complete E8 medium (Life technologies). We assessed the pluripotency of the iPS cells by differentiating them into embryoid bodies (EBs). iPSc clones were collected by collagenase treatment and resuspended in E8 medium without FGF2. Two weeks later, EBs were plated on polyornithine (20 µg/ml) and laminin (10 µg/ml)-coated cover slips and incubated for seven additional days. EBs were assessed for markers of the three germ layers: ectoderm (Nestin, Millipore), mesoderm (α-smooth muscle actin, Abcam), and endoderm (α-fetoprotein, Cell Signalling). iPS cells and EBS were also analyzed by real-time qPCR assays (TaqMan hPSC Scorecard Panel; Life Technologies) to confirm expression of pluripotency markers. iPS cells were differentiated into brain organoids following the protocol previously described (Pasca et al., 2015). After 90 days *in vitro*, organoids were fixed in 4% paraformaldehyde for 24 h, cryoconserved, and stored at -80°C. Organoid slices (12 µm) were cut on a cryostat (LEICA_CM3050S) and processed for immunostaining as described for the mouse brain slices. Images were obtained using a Leica SP-8 confocal microscope with a 60x objective (NA 1.4). Quantification of ganglioside accumulation was performed as for the mouse brain sections.

Primary cultures of neurons

Mouse primary cultures of cortical neurons were prepared as described (Branchu et al., 2017). When needed, neurons were treated with miglustat (Tocris) from the second day in culture. Medium was changed every three days. Vectors expressing miRNAs to downregulate GM3 synthase (GM3S), Neu1 and clathrin heavy chain (CHC) expression were produced using the Block-it kit (Life Technologies). The miRNA sequences were: ATGTACAGGAGCCAGACTCCAGTTTTGGCCACTGACTGACTGGAGTCTCTCCTGTACAT (miRNA GM3S-1), ATAACAGAGCCATAGCCGTCTGTTTTGGCCACTGACTGACAGACGGCTGGCTCTGTTAT (miRNA GM3S-2), TCTACAGAGCCGATCTGCTTCGTTTTGGCCACTGACTGACGAAGCAGAGGCTCTGTAGA (miRNA Neu1-1), CTACGATGAAGGCTGTAGAGGGTTTTGGCCACTGACTGACCCTCTACACTTCATCGTAG (miRNA Neu1-2), TATCAATGATTACCACCTGGGGTTTTGGCCACTGACTGACCCCAGGTGAATCATTGATA (miRNA CHC-1) and AATATTAGCTGACAGCATGGCGTTTTGGCCACTGACTGACGCCATGCTCAGCTAATATT (miRNA CHC-2). Neurons were transfected with vectors expressing the miRNA and GFP using the Neon transfection system (Life Technologies) with the following parameters: 1500V, 10ms, and 3 pulses. The efficiency of the miRNA sequences was validated by transfecting NIH-3T3 cells and performing quantitative RT-PCR using a LightCycler 480 apparatus (Roche) following the manufacturer's instructions.

For each replicate of lipidomic analysis, 10^6 neurons were grown in 100 cm^2 plate for six days *in vitro*. Neurons were washed twice in PBS, scraped and centrifuged at 5000g for 5 minutes. Dry pellet was kept at -80°C until samples were processed for lipidomic as detailed for lysosome-enriched fractions. The relative amount of GM2 was quantified as the area of its chromatographic peak, and it was normalized to the concentration of proteins in each pellet.

Immunostaining was performed after six days of culture *in vitro*, as previously described (Murmu et al., 2011), and images acquired using an Apotome2 microscope (Zeiss) with an objective Plan-Apochromat 63x

(N.A. 1.4), or with a Leica SP-8 confocal microscope. Ganglioside levels were quantified as the mean grey value using ImageJ. Colocalization of ganglioside staining with lysosomes was quantified using ImageJ on images of cultured neurons that were randomly chosen. First, we created a mask corresponding to Lamp1 staining using automatic threshold in Image J. The mask was copied to the corresponding fluorescence image of ganglioside. We quantified the total intensity of ganglioside fluorescence in the lysosome mask, and expressed it as the percentage of total ganglioside fluorescence in every neuron. A similar method was used to quantify the amount of clathrin colocalized with GM2 immunostaining. Live imaging of lysosome was performed on neurons transfected with a vector allowing expression of Lamp1-mCherry (Addgene, #45147) using a Yokogawa Confocal Spinning Disk module associated to a Leica DMi8 inverted microscope. For Cathepsin B activity assays, neurons were incubated with Magic Red™ Cathepsin B Assay Kit (1X according to manufacturer's instructions, ImmunoChemistry Technologies, #938) for 1h. Then, cells were fixed and stained with anti-α-tubulin and Alexa Fluor 488 secondary antibody. The average cathepsin B activity was monitored as the mean value of fluorescence measured with an automated ArrayScan XTI apparatus (Thermo-Fisher), using the general intensity measurement protocol. More than 1,500 cells were analysed per condition.

Neuronal death was induced by the addition of 200 µM glutamate (Sigma-Aldrich) in culture medium. To quantify neuronal death, 30 hours after glutamate treatment all neurons were labeled with 100 nM Cell tracker Deep Red (Life Technologies) and dead cells were labeled by propidium iodide (5 µM). The number of neurons positive for propidium iodide was quantified with an automated ArrayScan XTI apparatus using the compartmental analysis protocol.

Yeast two hybrid screen

The yeast two-hybrid screen was performed by Hybrigenics (Paris, France) with the 1943-2443 domain of human spatacsin as bait using an adult human cDNA brain library.

Coimmunoprecipitation

Hela cells were transfected with the Neon transfection system to express GFP-spatacsin (aa1943-2443). Cells were lysed in 100mM NaCl, 20mM Tris HCl, pH7.4, 1mM EDTA, 0.1% NP40 and complete inhibitor protease (Roche). GFP-spatacsin was immunoprecipitated using GFP-Trap beads (ChromoTek). Lysates and immunoprecipitates were separated by SDS-PAGE and immunoblotted onto nitrocellulose membranes. Western immunoblotting was performed with rabbit anti-GFP (Abcam) and mouse anti Dynamin (BD Biosciences) antibodies, and revealed using the West dura chemiluminescent substrate (Pierce).

Analysis of zebrafish model

Assessment of GM2 ganglioside levels in zebrafish larvae was performed at 48 hpf by whole-mount *in vivo* immunohistochemistry using 48 hpf embryos fixed in 4% paraformaldehyde in PBS for 2 h at room temperature. Embryos were washed 3 times in PBS-0.1% Triton X-100 (PBST). Embryos were blocked for 1 h in 5% normal goat serum in PBS containing 1% DMSO and 1% Triton X-100 (PBDT), then incubated overnight at 4 °C in PBDT containing the anti-GM2 primary antibody. After 4 washes in PBST, embryos were incubated with secondary antibody coupled to Alexa-488 (Thermo Fisher), overnight at room temperature in PBDT. Before observation, embryos were washed 3 times in PSBT and mounted in a drop of Fluoromount™ Aqueous Mounting Medium (Sigma Aldrich). Whole-mount embryos were imaged on a confocal microscope (Leica SP8, 40X, NA 0.8). Larvae were oriented in the same position for image capture to minimize potential biases in quantification. Image stacks were collected with a step-size of 0.35µm. Using ImageJ software, the maximum intensity projections of z-stacks were used for quantification of fluorescence in the telencephalon. Mean and variance of the fluorescence intensity were quantified for each morphant in a square of 100 pixels per 100 pixels. To quantify motor activity, we monitored the touch-evoked escape response at 48 hpf in larvae with no obvious developmental abnormalities as previously described (Martin et al., 2012). Images were acquired at 350 images per sec. Tracking of the touch evoked escape response was performed as previously described using the Image J manual tracking plugin (Fontaine et al., 2013).

Supplemental References

Branchu, J., Boutry, M., Sourd, L., Depp, M., Leone, C., Corriger, A., Vallucci, M., Esteves, T., Matusiak, R., Dumont, M., *et al.* (2017). Loss of spatacsin function alters lysosomal lipid clearance leading to upper and lower motor neuron degeneration. Neurobiol Dis 102, 21-37.

Dobrenis, K., Joseph, A., and Rattazzi, M.C. (1992). Neuronal lysosomal enzyme replacement using fragment C of tetanus toxin. Proc Natl Acad Sci U S A 89, 2297-2301.

Esteves, T., Durr, A., Mundwiller, E., Loureiro, J.L., Boutry, M., Gonzalez, M.A., Gauthier, J., El-Hachimi, K.H., Depienne, C., Muriel, M.P., *et al.* (2014). Loss of association of REEP2 with membranes leads to hereditary spastic paraplegia. Am J Hum Genet 94, 268-277.

Folch, J., Lees, M., and Sloane Stanley, G.H. (1957). A simple method for the isolation and purification of total lipides from animal tissues. J Biol Chem 226, 497-509.

Fontaine, R., Affaticati, P., Yamamoto, K., Jolly, C., Bureau, C., Baloche, S., Gonnet, F., Vernier, P., Dufour, S., and Pasqualini, C. (2013). Dopamine inhibits reproduction in female zebrafish (Danio rerio) via three pituitary D2 receptor subtypes. Endocrinology 154, 807-818.

Graham, J.M. (2001). Isolation of lysosomes from tissues and cells by differential and density gradient centrifugation. Curr Protoc Cell Biol Chapter 3, Unit 3 6.

Martin, E., Yanicostas, C., Rastetter, A., Naini, S.M., Maouedj, A., Kabashi, E., Rivaud-Pechoux, S., Brice, A., Stevanin, G., and Soussi-Yanicostas, N. (2012). Spatacsin and spastizin act in the same pathway required for proper spinal motor neuron axon outgrowth in zebrafish. Neurobiol Dis 48, 299-308.

Murmu, R.P., Martin, E., Rastetter, A., Esteves, T., Muriel, M.P., El Hachimi, K.H., Denora, P.S., Dauphin, A., Fernandez, J.C., Duyckaerts, C., *et al.* (2011). Cellular distribution and subcellular localization of spatacsin and spastizin, two proteins involved in hereditary spastic paraplegia. Mol Cell Neurosci 47, 191-202.

Natoli, E.J., Jr., Livingston, P.O., Pukel, C.S., Lloyd, K.O., Wiegandt, H., Szalay, J., Oettgen, H.F., and Old, L.J. (1986). A murine monoclonal antibody detecting N-acetyl- and N-glycolyl-GM2: characterization of cell surface reactivity. Cancer Res 46, 4116-4120.

Niemir, N., Rouviere, L., Besse, A., Vanier, M.T., Dmytrus, J., Marais, T., Astord, S., Puech, J.P., Panasyuk, G., Cooper, J.D., *et al.* (2018). Intravenous administration of scAAV9-Hexb normalizes lifespan and prevents pathology in Sandhoff disease mice. Hum Mol Genet 27, 954-968.

Okita, K., Matsumura, Y., Sato, Y., Okada, A., Morizane, A., Okamoto, S., Hong, H., Nakagawa, M., Tanabe, K., Tezuka, K., *et al.* (2011). A more efficient method to generate integration-free human iPS cells. Nature methods 8, 409-412.

Pasca, A.M., Sloan, S.A., Clarke, L.E., Tian, Y., Makinson, C.D., Huber, N., Kim, C.H., Park, J.Y., O'Rourke, N.A., Nguyen, K.D., *et al.* (2015). Functional cortical neurons and astrocytes from human pluripotent stem cells in 3D culture. Nature methods 12, 671-678.

Seyer, A., Boudah, S., Broudin, S., Junot, C., and Colsch, B. (2016). Annotation of the human cerebrospinal fluid lipidome using high resolution mass spectrometry and a dedicated data processing workflow. Metabolomics 12, 91.